Virtual reality-based real-time imaging reveals abnormal cortical dynamics during behavioral transitions in a mouse model of autism

Nakai, Nobuhiro ; Sato, Masaaki ; Yamashita, Okito ; Sekine, Yukiko ; Fu, Xiaochen ; Nakai, Junichi ; Zalesky, Andrew ; Takumi, Tooru

(Citation)
Cell Reports,42(4):112258

(Issue Date)
2023-04-25

(Resource Type)
journal article

(Version)
Version of Record

Cell Reports

Article

Virtual reality-based real-time imaging reveals abnormal cortical dynamics during behavioral transitions in a mouse model of autism

Graphical abstract

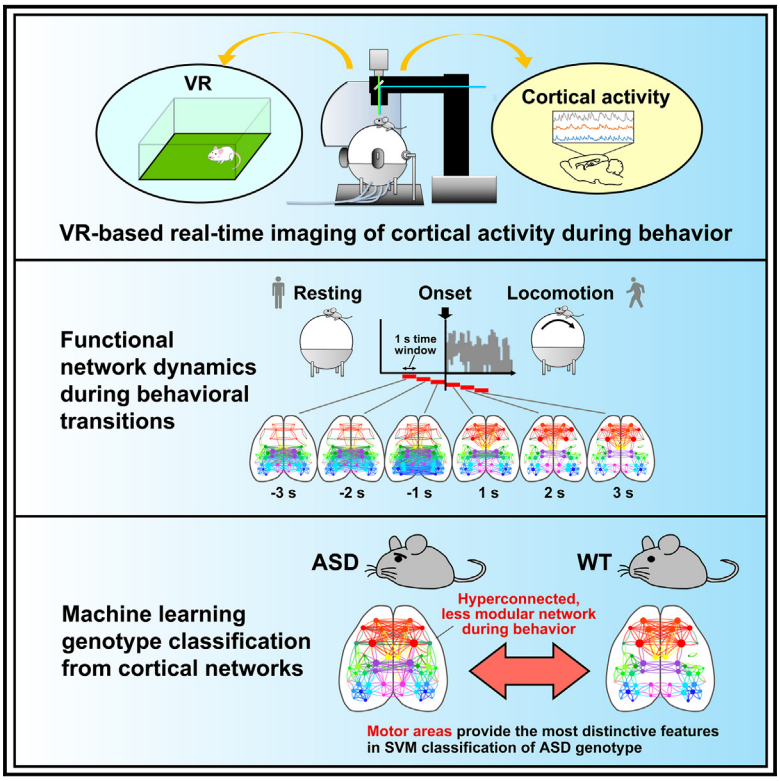

Highlights

- VR-based mesoscopic imaging reveals functional cortical networks during behavior
- Locomotion induces rapid reorganization and modularization of cortical networks
- *15q dup* ASD mice have hyperconnected, less modular cortical networks
- Motor areas provide contributing features for SVM classification of ASD genotype

Authors

Nobuhiro Nakai, Masaaki Sato, Okito Yamashita, ..., Junichi Nakai, Andrew Zalesky, Toru Takumi

Correspondence

msato@pop.med.hokudai.ac.jp (M.S.), takumit@med.kobe-u.ac.jp (T.T.)

In brief

Using virtual-reality-based mesoscopic Ca^{2+} imaging and graph analysis, Nakai et al. elucidate the rapid reorganization of widespread functional cortical networks during behavioral transitions in normal and ASD model mice. Machine learning identifies functional connectivity of motor areas as the most distinguishing feature for ASD genotype classification.

Nakai et al., 2023, Cell Reports *42*, 112258
April 25, 2023
https://doi.org/10.1016/j.celrep.2023.112258

CellPress

Cell Reports

CellPress
OPEN ACCESS

Article

Virtual reality-based real-time imaging reveals abnormal cortical dynamics during behavioral transitions in a mouse model of autism

Nobuhiro Nakai,[1,2] Masaaki Sato,[1,3,*] Okito Yamashita,[4,5] Yukiko Sekine,[1] Xiaochen Fu,[1] Junichi Nakai,[6] Andrew Zalesky,[7] and Toru Takumi[1,2,8,9,*]

[1]RIKEN Brain Science Institute, Wako, Saitama 351-0198, Japan
[2]Department of Physiology and Cell Biology, Kobe University School of Medicine, Chuo, Kobe 650-0017, Japan
[3]Department of Neuropharmacology, Hokkaido University Graduate School of Medicine, Kita, Sapporo 060-8638, Japan
[4]RIKEN Center for Advanced Intelligence Project, Chuo, Tokyo 103-0027, Japan
[5]Department of Computational Brain Imaging, ATR Neural Information Analysis Laboratories, Seika, Kyoto 619-0288, Japan
[6]Division of Oral Physiology, Department of Disease Management Dentistry, Tohoku University Graduate School of Dentistry, Aoba, Sendai 980-8575, Japan
[7]Melbourne Neuropsychiatry Centre and Department of Biomedical Engineering, The University of Melbourne, Melbourne, VIC 3010, Australia
[8]RIKEN Center for Biosystems Dynamics Research, Chuo, Kobe 650-0047, Japan
[9]Lead contact
*Correspondence: msato@pop.med.hokudai.ac.jp (M.S.), takumit@med.kobe-u.ac.jp (T.T.)
https://doi.org/10.1016/j.celrep.2023.112258

SUMMARY

Functional connectivity (FC) can provide insight into cortical circuit dysfunction in neuropsychiatric disorders. However, dynamic changes in FC related to locomotion with sensory feedback remain to be elucidated. To investigate FC dynamics in locomoting mice, we develop mesoscopic Ca^{2+} imaging with a virtual reality (VR) environment. We find rapid reorganization of cortical FC in response to changing behavioral states. By using machine learning classification, behavioral states are accurately decoded. We then use our VR-based imaging system to study cortical FC in a mouse model of autism and find that locomotion states are associated with altered FC dynamics. Furthermore, we identify FC patterns involving the motor area as the most distinguishing features of the autism mice from wild-type mice during behavioral transitions, which might correlate with motor clumsiness in individuals with autism. Our VR-based real-time imaging system provides crucial information to understand FC dynamics linked to behavioral abnormality of neuropsychiatric disorders.

INTRODUCTION

Neocortical activity displays dynamic changes across multiple cortical areas to facilitate processing of sensory information and generate action outputs.[1] Such large-scale network dynamics can be investigated using functional connectivity (FC), defined as temporal dependence of neuronal activity between anatomically separated brain regions.[2] With functional magnetic resonance imaging (fMRI), FC is quantified as the extent of coactivation between spontaneous blood-oxygen-level-dependent (BOLD) signals during rest or task conditions necessitating minimal movement.[2,3] FC can also be measured in rodents.[4] However, the immobilization of a subject within an MRI scanner and the slow nature of BOLD signals in resting-state fMRI has limited the study of cortical activity during complex behaviors involving whole-body movement and locomotion. Although the ability to record sensory-evoked BOLD signals in awake head-restrained mice was recently developed,[5] techniques to measure FC during natural and voluntary movement in an interactive environment remain to be established.

FC provides a valuable tool for investigating functional brain network organization in autism spectrum disorder (ASD).[6] A large body of resting-state fMRI studies reports functional under-connectivity (hypoconnectivity), over-connectivity (hyperconnectivity), and a combination of global and local alterations in the ASD brain.[7] In addition, machine learning models can be trained to predict an individual's diagnostic status using their FC, although clinical heterogeneity is a significant challenge.[8,9] In contrast to resting-state and task conditions, cortical dynamics during voluntary behaviors such as locomotion remain to be understood, particularly in neuropsychiatric disorders. Individuals with ASD exhibit motor coordination deficits[10] and impairment of movement planning in goal-directed locomotion.[11,12] Furthermore, accumulating evidence suggests that sensorimotor difficulties seen in ASD are strongly associated with the development and maintenance of social and non-social core symptoms.[13]

In this study, we sought to elucidate the rapid reorganization of functional cortical networks during locomotion, focusing on periods transitioning between locomotion (i.e., running) and rest conditions, in normal and ASD model mice. To this end, we

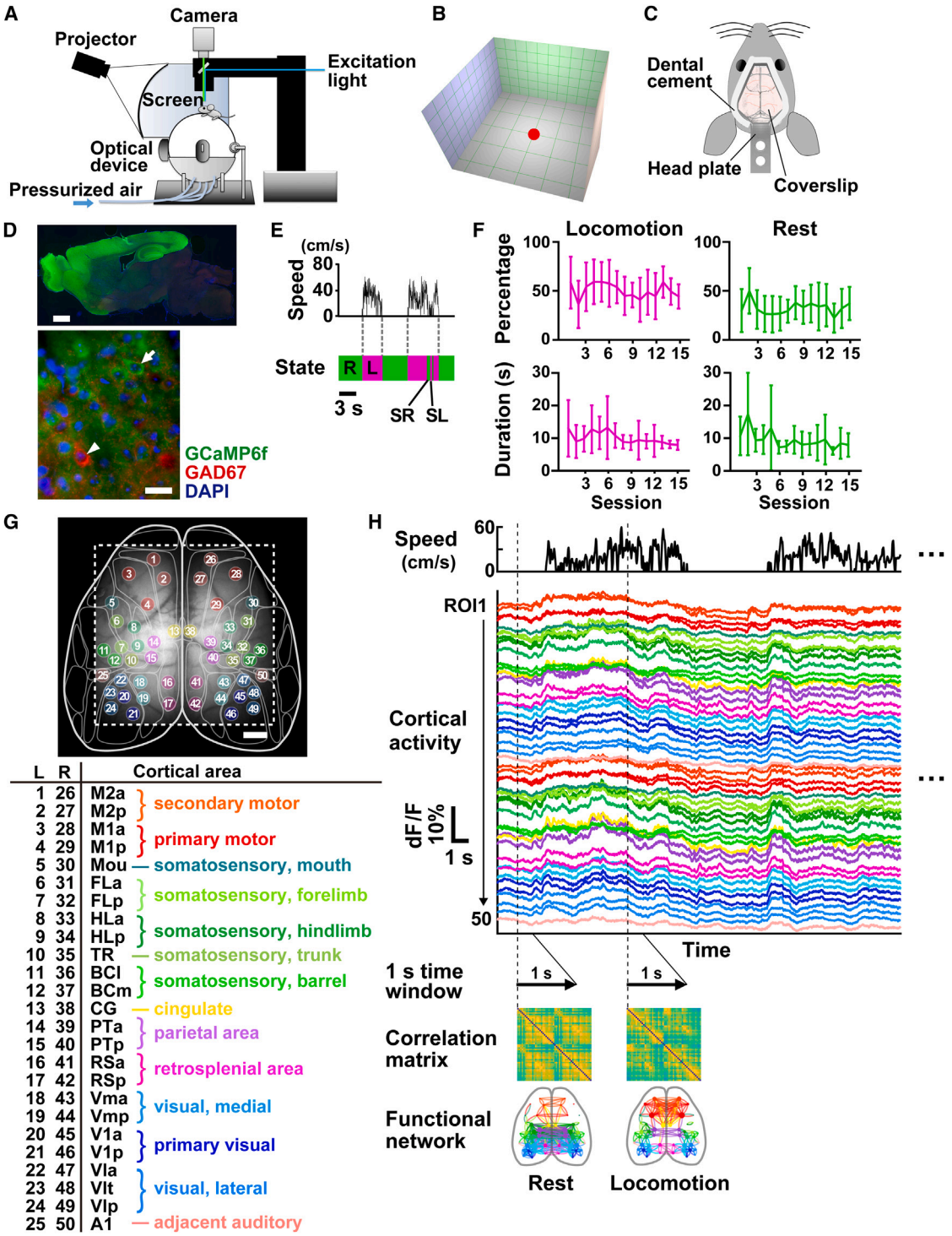

Figure 1. Analysis of cortical FC with mesoscopic Ca^{2+} imaging

(A) The imaging and virtual reality (VR) system.

(B) The virtual arena. The floor and walls have green gridlines to enhance the sense of visual flow. Each wall is painted in a different color. The mouse starts to move from the location indicated by the red dot.

(C) A schematic of the transcranial imaging window affixed to the mouse skull.

(legend continued on next page)

developed an integrated Ca^{2+} imaging and virtual reality (VR) platform to study neural activity in mice during VR locomotion, including statistical analysis of second-by-second FC dynamics, graph theoretical analysis of network structures, and machine learning classification of FC patterns using a support vector machine (SVM). Cortex-wide mesoscopic Ca^{2+} imaging enabled the measurement of neural activity with high spatiotemporal resolution.[14,15] VR created an environment that simulated real-world situations for head-fixed mice and allowed us to manipulate sensory information.[16,17] Using this experimental and analytical framework, we assessed cortical FC of a copy number variation mouse model for human 15q11-13 duplication (*15 dup*) in different behavioral states. We previously reported that *15q dup* mice display ASD-like social communication deficits[18,19] and exhibit abnormal somatosensory tuning under anesthesia and whole-brain functional hypoconnectivity in awake resting-state fMRI.[5,20] However, cortical FC alterations during behavior remain unknown. Here, we found that these mice exhibited impaired locomotion-dependent FC dynamics and aberrant FC patterns involving hyperconnectivity of the motor areas, highlighting the importance of motor areas in cortical FC dysfunction during spontaneous behavioral switching in ASD.

RESULTS

To measure cortical FC in mice engaged in voluntary movement, we used transcranial Ca^{2+} imaging combined with a head-fixed VR system (Figures 1A–1C; STAR Methods). The virtual environment mimicked a realistic open-field enclosure and consisted of a two-dimensional square arena with differently colored walls (Figure 1B). We crossed Emx1-Cre driver mice, which allow extensive Cre-mediated recombination in the forebrain, with Ai95D mice to express the genetically encoded calcium indicator GCaMP6f in cortical excitatory neurons of the offspring Emx1G6 mice (Figure 1D; STAR Methods). During a 10-min VR session, mice exhibited voluntary locomotion (speed >0.5 cm/s) in this virtual arena; they spent 58.7% ± 19.7% of the total duration in a state of locomotion (mean ± SD, n = 89 sessions from seven mice). For further analysis, we excluded periods of frequent alterations between locomotion and rest and focused only on long episodes (continuously ≥3 s) of locomotion and rest (Figure 1E). The percentage of time spent in long locomotion and rest was 50.3% ± 22.1% and 32.5% ± 20.2%, respectively (mean ± SD, n = 89 sessions from seven mice). Average lengths of long locomotion and rest episodes were 10.0 ± 5.4 s (mean ± SD, n = 2,836 episodes from 89 sessions) and 9.4 ± 6.6 s (mean ± SD, n = 1,903 episodes from 89 sessions), respectively. There were no significant changes in these behavioral parameters across sessions (Figure 1F). We imaged cortical fluorescence changes at a frame rate of 30 frames per second in 50 regions of interest (ROIs) that covered most of the dorsal cortical subregions (Figure 1G and 1H; Figures S1 and S2; STAR Methods). Pairwise correlation coefficients were computed between cortical ROIs at a temporal scale of a second using a one-frame sliding window. We then applied graph-theoretic analyses to characterize the resulting network dynamics and visualized highly correlated ROI pairs ($r > 0.8$) using an FC map (Figure 1H; STAR Methods).

Graph analysis of cortical network dynamics during behavioral transitions

First, we examined the activity of different cortical areas during behavioral transitions from long rest to long locomotion (locomotion onset, n = 566 events from 89 sessions) and from long locomotion to long rest (locomotion cessation, n = 643 events from 89 sessions; Figure 2A). During a period that spanned 3 s before and after the onset of locomotion, many cortical areas displayed marked transient increases in fluorescence intensity that began slightly prior to the onset (dF/F; 0.05% ± 0.27% at −0.5 s; 0.62% ± 0.45% at 0 s; n = all 50 ROIs, mean ± SD; Figure 2A). In contrast, the fluorescence intensity of all areas rapidly and substantially decreased immediately after the cessation of locomotion (−0.06% ± 0.12% at 0 s; −0.54% ± 0.34% at 0.5 s). Such large signal changes were not observed during control periods that were randomly selected independent of the locomotion state (−0.01% ± 0.03% at −0.5 s; −0.03% ± 0.04% at 0 s; 0.01% ± 0.03% at 0.5 s). Hierarchical clustering of regional fluorescence signals revealed that response profiles of all ROIs during the onset periods could be divided into two major clusters: one represented the considerable transient activity of sensory (primary visual [V1], somatosensory, hindlimb [HL], somatosensory, forelimb [FL], etc.) and association (HL, parietal area [PT],

(D) Expression of GCaMP6f in a parasagittal section of an adult Emx1G6 mouse (top, scale bar, 1 mm). Immunofluorescence detection of GCaMP6f (green) and GAD67 (red) in layer 2/3 of the primary motor cortex (bottom, scale bar, 20 μm). Cell nuclei were stained with DAPI (blue). The arrow and arrowhead indicate an example of GCaMP6f-positive cells and GAD67-positive cells, respectively.

(E) Two behavioral states, long locomotion (L) and long rest (R), were defined by spontaneous locomotion and resting states (duration ≥ 3 s) of head-fixed mice. Locomotion and rest episodes shorter than 3 s, short locomotion (SL) and short rest (SR), were excluded from FC analysis during behavioral transitions.

(F) Percentages of time spent in long locomotion and long rest (top) and average lengths of long locomotion and long rest episodes (bottom) across sessions. Data represent mean ± SD. (Percentage) locomotion, $F_{(14, 74)} = 0.61$, p = 0.84; rest, $F_{(14, 74)} = 0.52$, p = 0.91. (Duration) locomotion, $F_{(14, 74)} = 0.63$, p = 0.83; rest, $F_{(14, 74)} = 1.83$, p = 0.58, n = 11–15 sessions/mouse, seven mice, one-way ANOVA.

(G) Fifty cortical ROIs are overlaid onto a gray-scale image of the dorsal cortex with a cortical parcellation map (top, dashed lines indicate the field of view; scale bar, 1 mm). ROIs 1–25 and 26–50 were defined in the left (L) and right (R) hemispheres, respectively, and ROIs for each hemisphere are numbered along the anterior-posterior axis (bottom). The lowercase letters following cortical areas indicate anterior (e.g., secondary motor, anterior [M2a]) and posterior (e.g., M2p) or lateral (e.g., somatosensory, lateral barrel [BCl]) and medial (e.g., BCm) positions.

(H) Analysis of cortical FC. After calculating normalized fluorescence changes (dF/F) for each ROI, pairwise Pearson's correction coefficients of cortical activity in a 1-s time window were calculated for all ROI pairs and then visualized as matrices. Each matrix was labeled with a corresponding behavior state at the first frame of the time window. In graph visualization of functional networks, connectivity with a correlation coefficient above a threshold ($r > 0.8$) was denoted as a line (edge) that connected the corresponding ROIs (nodes).

See also Figure S1.

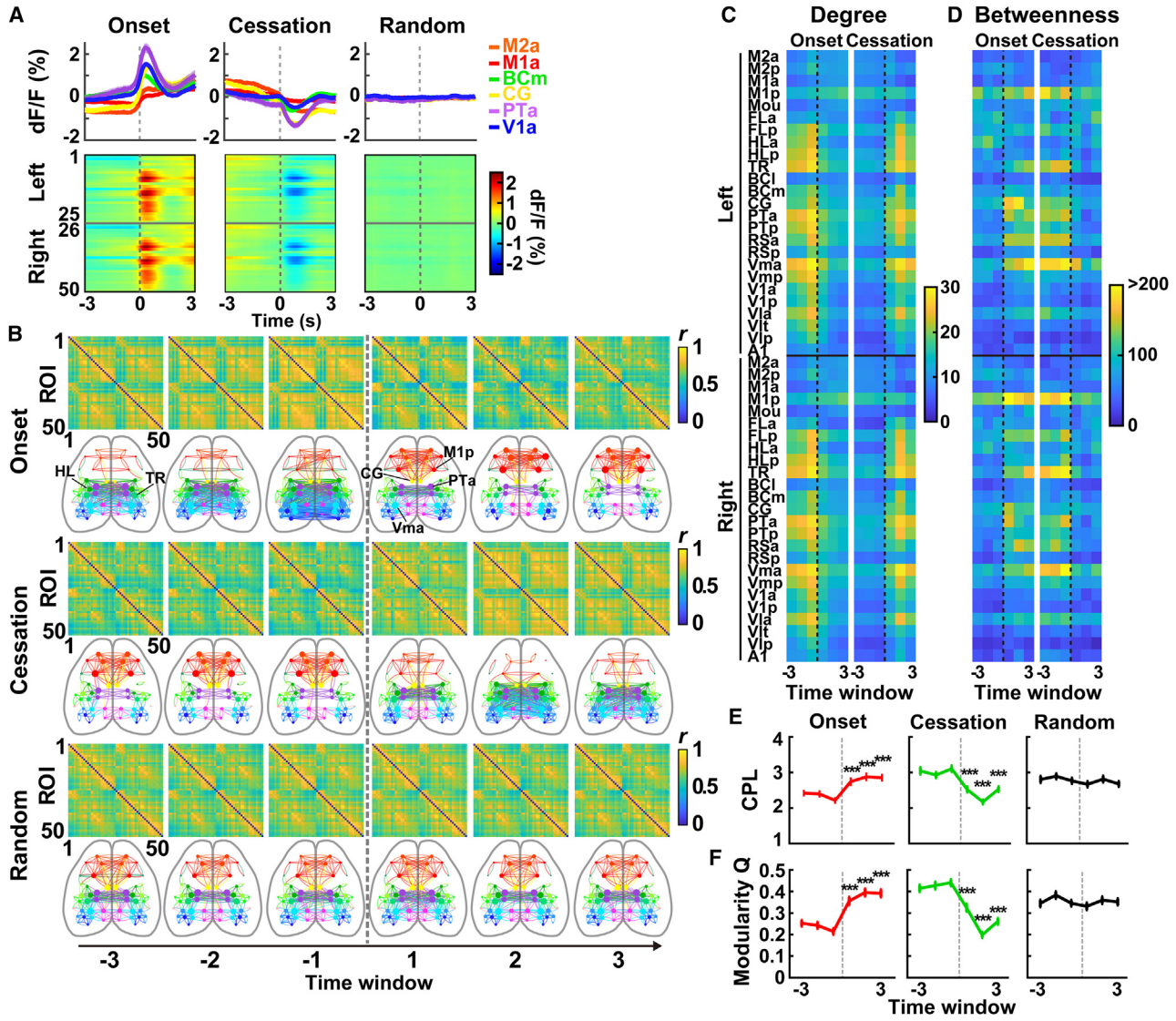

Figure 2. Dynamic reconfiguration of the functional cortical network during behavioral transitions

(A) Cortical activity during behavioral transitions in Emx1G6 mice. The top plots present average relative changes in fluorescence signals in representative cortical areas (n = 89 sessions from seven mice). The vertical dashed lines indicate the occurrence of transition. The colormaps at the bottom show changes in fluorescence signals in all ROIs. ROI 1–25 and 26–50 were defined in the left and right hemispheres, respectively (see Figure 1G for details).

(B) Dynamics of the functional cortical network during the behavioral transitions. The data for locomotion onset, cessation, and random control are shown from top to bottom. Correlation matrices and FC graphs ($r > 0.8$) were determined for each second of the time window encompassing the relevant behavioral transition that occurred at time zero (vertical dashed line). Time windows −3, −2, −1, 1, 2, and 3 correspond to windows that cover −3 to −2 s, −2 to −1 s, −1 to 0 s, 0 to 1 s, 1 to 2 s, and 2 to 3 s, respectively.

(C and D) Changes in node degree (C) and betweenness centrality (D) during the transitions.

(E) Change in characteristic path length (CPL) during the transitions. Data represent mean ± SEM. Onset, $F_{(5,\ 612)} = 11.35$, $p = 1.7 \times 10^{-10}$; cessation, $F_{(5,\ 600)} = 19.15$, $p = 1.1 \times 10^{-17}$; random, $F_{(5,\ 612)} = 0.22$, $p = 0.95$, one-way ANOVA. ***$p < 0.001$ vs. time window −1, Tukey-Kramer test, n = 89 sessions from seven mice.

(F) Change in modularity Q during the transitions. Data represent mean ± SEM. Onset, $F_{(5,\ 612)} = 25.46$, $p = 2.3 \times 10^{-23}$; cessation, $F_{(5,\ 600)} = 37.20$, $p = 3.0 \times 10^{-23}$; random, $F_{(5,\ 612)} = 0.51$, $p = 0.77$, one-way ANOVA. ***$p < 0.001$ vs. time window −1, Tukey-Kramer test, n = 89 sessions from seven mice.

See also Figures S3 and S4.

retrosplenial area [RS], etc.) areas and the other represented sustained activity of the motor-related regions (primary motor [M1], M2, etc.; Figure S3A). On the other hand, the clustering of activity around the locomotion cessation differentiated M2 and cingulate [CG] from the major clusters (Figure S3B).

Next, we investigated cortical FC dynamics during transition periods by visualizing indices that represent the network centrality of each cortical area. Node degree captures the extent to which a region connects with other regions. Betweenness centrality measures how much a region is in between other regions.[21] Before

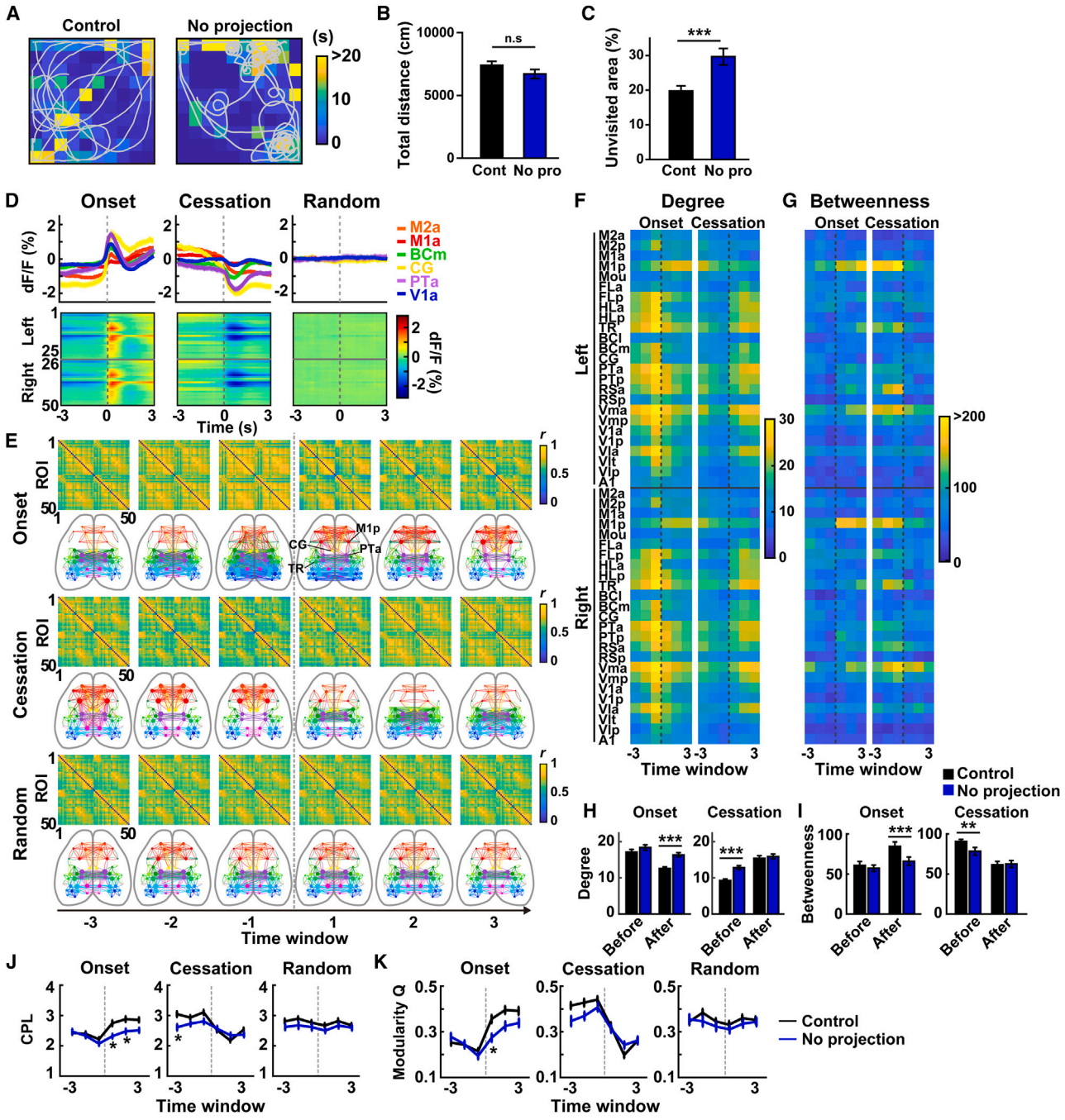

Figure 3. Changes in behavior and functional cortical network during exploration without visual information

(A) Representative trajectories overlaid onto heatmaps of dwell time during exploration with (Control) and without (No projection) visual information.

(B and C) Distance traveled (B) and percentage of unvisited areas (C) during 10-min sessions with (Cont) or without (No pro) visual information. Data represent mean ± SEM. n.s., p = 0.14; ***p < 0.001; t test; n = 89 control sessions from seven mice and 71 no-projection sessions from 17 mice.

(D) Cortical activity of Emx1G6 mice without visual information. The convention of the figure is the same as in Figure 2A.

(E) Dynamics of correlations between activities of ROI pairs during the behavioral transitions without visual information. FC graphs ($r > 0.8$) were generated using the data shown in (D). The convention of the figure is the same as in Figure 2B.

(F and G) Changes in node degree (F) and betweenness centrality (G) during the transitions in each ROI.

(H and I) Mean node degree (H) and mean betweenness centrality (I) during the transitions. Data across all ROIs were averaged. **p < 0.01, ***p < 0.001, t test, n = 89 control sessions from seven mice and 71 no-projection sessions from 17 mice.

(J and K) Change in CPL (J) and modularity Q (K) during the transitions. The control data presented in Figure 2 are again shown in black for comparison. Data represent mean ± SEM. (CPL) Onset, time, $F_{(5, 930)} = 11.95$, p = 3.1 × 10^{-11}; condition, $F_{(1, 930)} = 22.28$, p = 2.7 × 10^{-6}; time × condition, $F_{(5, 930)} = 2.68$, p = 0.02.

(legend continued on next page)

locomotion onset, FC among posterior areas (blue and green edges), most notably bilateral HL, somatosensory, trunk (TR), PT, and Vm, gradually increased (time window from −3 to −1; Figure 2B top), and node degree also increased in many areas (15.8 ± 5.9 at −3 s; 20.9 ± 6.3 at −1 s; n = all 50 ROIs, mean ± SD; Figure 2C). At locomotion onset, FC among posterior regions rapidly decreased, and highly correlated networks among anterior motor areas (orange and red edges) subsequently emerged (Figure 2B top). The node degree of most areas rapidly declined after locomotion onset (15.4 ± 3.6 at 1 s, n = all 50 ROIs, mean ± SD), although the primary motor area remained elevated (M1p, 13.5 ± 0.7 at −3 s; 16.7 ± 0.7 at −1 s; 17.7 ± 0.1 at 1 s, n = 2 ROIs; Figure 2C). At the cessation of locomotion, the dense anterior networks among motor areas disappeared, and the FC among posterior regions reemerged (Figure 2B middle). These locomotion-dependent dynamic reconfigurations of functional network architecture were absent during random control periods (Figure 2B bottom). Taken together, the results demonstrate that the correlation among anterior motor areas becomes dominant over posterior sensory/association cortices during locomotion, whereas this reciprocal relationship between anteroposterior cortical domains is reversed during rest.

The betweenness centrality of M1p remained high during locomotion (Figure 2D), consistent with the notion that the primary motor area plays a pivotal role in voluntary movement. In addition, the betweenness centrality of the CG and PTa increased rapidly at locomotion onset, and PTa was high again immediately before the cessation of locomotion. In contrast, TR and Vma displayed delayed rises after the onset and peaked immediately before cessation (Figure 2D). Fluorescence changes of each ROI were significantly correlated with node degree but not with betweenness centrality before locomotion onset (Figure S4), indicating that these functional network properties do not directly reflect the magnitude of fluorescence changes. These findings suggest that locomotion onset and cessation do not necessarily mirror each other, and hub structure dynamically changes within the period of locomotion. Moreover, we found significant increases in characteristic path length (CPL), a measure of the efficiency of information transfer that represents the average shortest path length between all region pairs (Figure 2E), and modularity Q, which means the extent to which the network is subdivided into non-overlapping groups of regions (Figure 2F). These findings suggest that functional cortical networks manifest a more modular structure during movement than during rest periods of no locomotion. We found that correction for hemodynamic signals did not significantly affect these findings (Figure S5).

Role of visual information in behavioral state-dependent cortical network dynamics

Animals use visual information to explore external environments. To investigate the role of visual sensory processing on our results, we tested mice exploring a virtual environment with no projection of visual landscape (Figure 3). In this condition, mice spent 46.9% ± 24.8% and 35.2% ± 24.6% of total time engaged in long locomotion and rest, respectively (mean ± SD; long locomotion, p = 0.38 vs. control; long rest, p = 0.46 vs. control, t test, n = 71 sessions from 17 mice). Total distances traveled did not differ significantly from the control experiments with projection (Figure 3B). However, the mice often exhibited local circling and were impeded by invisible walls and corners when they explored without visual information (Figure 3A). As a result, they traversed a significantly smaller area within the arena (Figure 3C). These results demonstrate that vision provides important sensory information when mice explore the virtual arena.

We then examined FC dynamics under no visual information. The fluorescence changes at locomotion onset and cessation were comparable with those in the control experiments except for larger and smaller amplitudes in CG (mean ± SD; 136.8% ± 34.0% vs. control, n = 71 sessions from 17 mice) and V1a (67.1% ± 19.9%), respectively (Figures 3D and 2A). While FC networks were similar to those in the control experiments (Figures 3E and 2B), the number of connections during locomotion was significantly higher under no projection (Figures 3F, 3H, and 2C). As in control experiments, the betweenness centrality of M1p was constantly high during locomotion. However, these centralities of CG, TR, and Vma were substantially reduced (no projection, 102.8 ± 41.7; control, 145.5 ± 33.7; mean ± SD, n = 6 ROIs; Figures 3G and 2D), which led to significant decreases in overall betweenness centrality during locomotion (Figure 3I). Furthermore, CPL and modularity Q were also significantly reduced after locomotion onset (Figures 3J and 3K), although significantly lower overall CPL observed in random control may have at least partly contributed to the reduction of locomotion-elicited CPL increase (Figure 3J, see figure legend for details). These results indicate that the lack of visual information markedly weakens the network modularity of locomotion-dependent cortical FCs.

Desynchronization of cortical population activity often manifests when animals engage in a task.[22] Using the network-based statistic (NBS),[23] we next tested for changes in FC during transitions between rest and locomotion. Importantly, this analysis allowed us to identify FCs that exhibited not only significantly higher correlations but also significantly lower correlations (i.e., decorrelation). In the control experiments, we observed gradual and marked increases in FC among posterior sensory areas and the emergence of decorrelated subnetworks of anterior motor areas before locomotion onset (time window from −3 to −1; Figure 4A). After locomotion began, long-range decorrelations among anterior (motor areas), parietal (CG), and posterior (visual areas) cortices rapidly emerged, followed by robust decorrelations among posterior sensory cortices 2–3 s after locomotion onset (Figure 4A). In contrast, persistently decorrelated subnetworks of posterior sensory cortices during locomotion expanded to include M2 immediately before locomotion cessation, followed by the emergence of sustained decorrelations among

Cessation, time, $F_{(5, 924)} = 19.59$, $p = 1.4 \times 10^{-18}$; condition, $F_{(1, 924)} = 9.47$, $p = 0.002$; time × condition, $F_{(5, 924)} = 3.29$, $p = 0.006$; random, time, $F_{(5, 948)} = 1.25$, $p = 0.28$; condition, $F_{(1, 948)} = 9.65$, $p = 0.002$; time × condition, $F_{(5, 948)} = 0.12$, $p = 0.99$; (modularity Q) onset, time, $F_{(5, 930)} = 29.78$, $p = 4.0 \times 10^{-28}$; condition, $F_{(1, 930)} = 11.03$, $p = 9.3 \times 10^{-4}$; time × condition, $F_{(5, 930)} = 3.19$, $p = 0.007$; cessation, time, $F_{(5, 924)} = 44.90$, $p = 1.5 \times 10^{-41}$; condition, $F_{(1, 924)} = 4.37$, $p = 0.04$; time × condition, $F_{(5, 924)} = 2.94$, $p = 0.01$; random, time, $F_{(5, 948)} = 1.45$, $p = 0.20$; genotype, $F_{(1, 948)} = 2.78$, $p = 0.10$; time × condition, $F_{(5, 948)} = 0.42$, $p = 0.83$, two-way ANOVA. *$p < 0.05$ vs. control, Tukey-Kramer test. n = 89 control sessions from seven mice and 71 no-projection sessions from 17 mice.

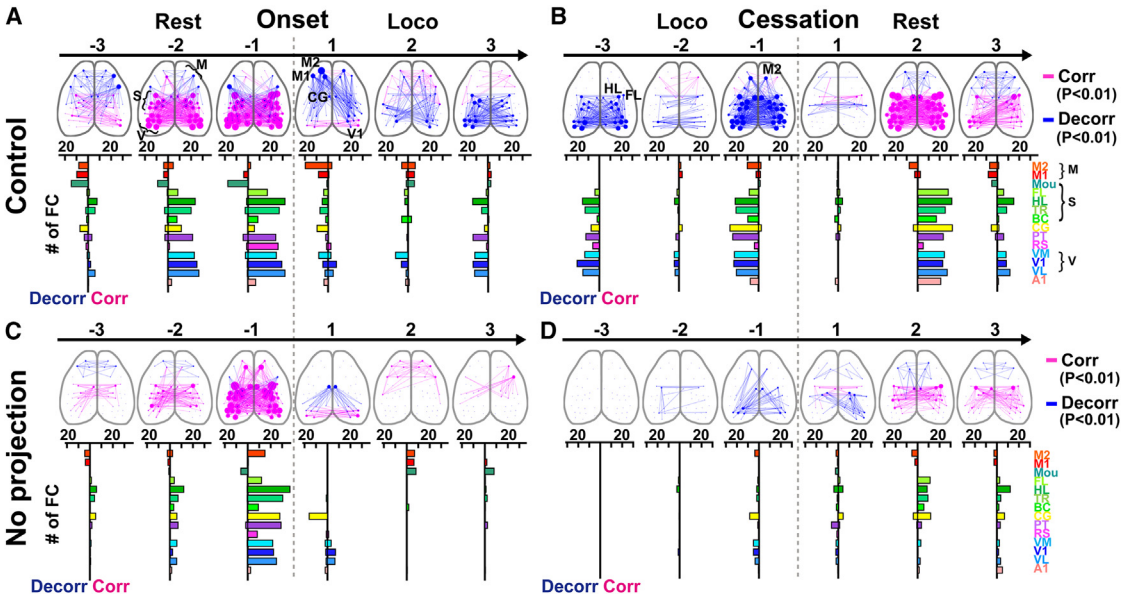

Figure 4. Statistically significant correlations and decorrelations within functional cortical networks during behavioral transitions with or without visual information

(A and B) Significant correlations and decorrelations of functional cortical subnetworks of Emx1G6 mice during locomotion onset in control experiments (A). Network diagrams of statistically significant FC during each second before and after the locomotion onset are shown from left to right (top). Magenta and blue lines denote significant correlations (Corr) and decorrelations (Decorr) compared with the random control, respectively. The horizontal bar plots (bottom) indicate the number of significant FC (rightward, Corr; leftward, Decorr) connected to each cortical area. The cortical areas are sorted along the antero-posterior axis from top to bottom. The values were averaged across bilateral ROIs and further averaged across multiple ROIs if the area contained more than one ROI. The same convention applies to locomotion cessation (B). Loco, locomotion; M, motor areas; S, somatosensory areas; V, visual areas. $p < 0.01$, NBS. n = 89 sessions from seven mice.

(C and D) Significant correlations and decorrelations of functional cortical subnetworks during locomotion onset (C) and cessation (D) in Emx1G6 mice under no projection of visual landscape. $p < 0.01$, NBS. n = 71 sessions from 17 mice.

See also Figure S8.

anterior motor cortices and widespread transient correlations among posterior sensory cortices beginning 1–2 s after cessation (Figure 4B). It is noteworthy that the number and distribution of significantly altered FCs exhibited apparent interhemispheric differences in some maps (e.g., FL at 1 s before and M2 at 1 s after locomotion onset and FL, HL, and TR at 3 s after locomotion cessation; Figure S8A).

The emergence of dense (de)correlated networks among sensory areas during behavioral transitions suggests that sensory processing could profoundly affect FC during these periods. Interestingly, we found that the decorrelated but not correlated networks markedly diminished in the condition with no projection of visual landscape (Figure 4C and 4D). Rapid decorrelations between M2 and V1 at ~1 s after locomotion onset and delayed decorrelations among posterior sensory areas, including not only visual but also somatosensory cortices, at ~3 s after locomotion onset were almost absent (Figure 4C), although decorrelations between CG and V1 and correlations between bilateral visual areas at ~1 s after locomotion onset remained. Persistent decorrelations among posterior sensory areas before cessation and transient correlations among those areas ~2 s after the cessation were considerably weakened (Figure 4D). Moreover, the interhemispheric differences were less evident than the control condition except for a few areas (e.g., CG at 3 s before onset and 3 s after cessation and somatosensory, mouth [Mou] at 3 s after onset; Figure S8B). Collectively, these results demonstrate that the absence of visual information markedly alters exploration behavior and dynamics of multiple functional subnetworks primarily involving the visual cortex, such as long-range antero-posterior FCs between motor and visual cortices and cross-modal FCs between somatosensory and visual cortices.

Decoding behavioral dynamics using a functional cortical network

Having found that the transitions between states of rest and locomotion were each characterized by distinct cortical network architectures, we tested whether an animal's behavioral state can be decoded from its cortical network. To this end, we trained SVM classifiers using datasets of FC containing all time frames from four mice (train set) and classified FCs for the remaining three mice (test set) into two behavioral states. This was repeated for all combinations of mouse assignments to test and train sets. Accuracy of the out-of-sample classification (Test, 88.9%, median, n = 35 classifiers) was comparable with the level achieved by classification for the train set (Train, 89.0%) and substantially higher than expected due to chance, as determined by randomly shuffling classification labels (Shuffled, 58.3%; Figure 5A). Incorrect classification mainly occurred during short periods flanking the state transition, and classification accuracy was highest during continuing locomotion and rest

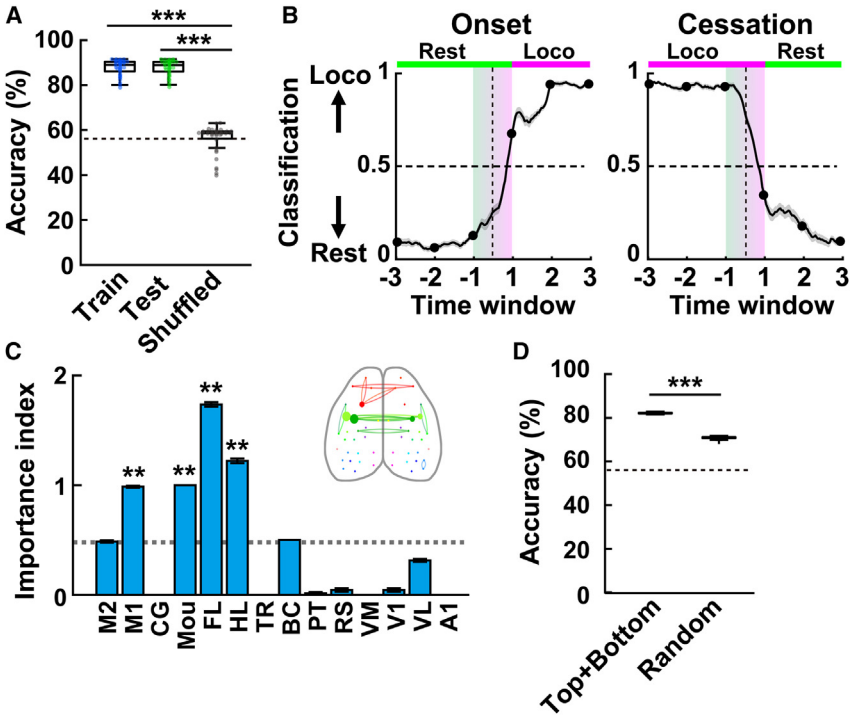

Figure 5. Decoding behavioral states from the functional cortical network on a subsecond timescale

(A) Accuracy of SVM classification of FC into the two behavioral states. The results of classification for train set (Train), test set (Test), and shuffled control are shown. Data represent averages across entire sessions (n = 35 classifiers, 17,970-time points each). The boxes represent the 25th, 50th, and 75th percentiles, and the whiskers represent the range except for outliers. The dashed line indicates the chance level defined as an overall average of time spent in locomotion (58.7%). ***p < 0.001 vs. shuffled. Wilcoxon rank-sum test with Bonferroni correction.

(B) Dynamics of SVM classification of FC during locomotion onset and cessation. The y axis indicates the classification index (1, classified into locomotion state; 0, classified into resting state). The magenta and green bars on the top indicate the periods during locomotion (Loco) and rest, respectively. The gradation bar from −1 to 1 indicates that the time window during this period contained FC from both locomotion and rest periods. Data represent mean ± SEM (n = 35 classifiers).

(C) Importance index of each cortical area. The index was defined as the number of the appearance of FCs connected to each area in the top 0.5% and bottom 0.5% features (see STAR Methods for details). The dashed line indicates a chance level defined as an average of 100-times random sampling of 1% features. (Inset) FCs that appeared frequently in the top 0.5% and bottom 0.5% features (>50% of total 35 classifiers). **p < 0.01 vs. chance level. Wilcoxon rank-sum test with Bonferroni correction. n = 35 classifiers each.

(D) Classification accuracy using the top 0.5% and bottom 0.5% features (Top + Bottom) and randomly selected 1% features (Random). ***p < 0.001. Wilcoxon rank-sum test. n = 35 classifiers each.

periods. However, accuracies remained modest during the intermediate periods in which two contrasting states coexisted (time window from −1 to 1; Figure 5B). Accordingly, the accuracy of classification increased to 92.3% (n = 1,326,379 frames from 89 sessions) when the periods of short locomotion episodes and short rest episodes (less than 3 s) were excluded, whereas accuracy within the periods of short episodes was 65.0% (n = 275,621 frames from 89 sessions).

To identify the features that contributed significantly to the classification, we sorted all FCs according to feature weights and found that M1, Mou, FL, and HL were significantly over-represented in the top 0.5% and bottom 0.5% of FCs (six FCs each) (Figure 5C). We then retrained the classifiers using these top 0.5% and bottom 0.5% of FCs and achieved classification accuracies that were comparable with the classifier trained with all FCs (Top + Bottom, 84.2%; Figure 5D) and significantly better than the classifiers trained with a randomly selected 1% of all FCs (Random, 71.0%; Figure 5D). Collectively, these results demonstrate that connectivity of the primary motor and primary somatosensory forelimb, hindlimb, and mouth areas contains information sufficient for highly accurate differentiation of locomotion and rest states.

Functional hyperconnectivity and impaired locomotion-dependent dynamics in the cortex of a mouse model of ASD

We applied our VR-based imaging system to the investigation of behavior-dependent cortical network dynamics of ASD model mice. We used Emx1G6$_{15q\ dup}$ mice that possessed the paternal duplication of the mouse syntenic region of human 15q11-13 and expressed GCaMP6f in excitatory neurons in the cortex. Emx1G6$_{15q\ dup}$ mice showed lower locomotor activity in the virtual arena during 10-min sessions (Figures 6A and 6B). They spent 25.8% ± 17.1% and 59.1% ± 21.3% of total time engaged in long locomotion and rest, respectively (mean ± SD; long locomotion, $p = 5.3 \times 10^{-14}$ vs. Emx1G6; long rest $p = 6.9 \times 10^{-15}$ vs. Emx1G6; t test, n = 88 sessions from nine mice; Figure 6C), and average lengths of long locomotion and rest per episode were 9.0 ± 4.2 s (p = 0.17 vs. Emx1G6, t test, n = 1,523 episodes from 88 sessions) and 20.5 ± 14.7 s ($p = 2.7 \times 10^{-9}$ vs. Emx1G6, t test, n = 1,882 episodes from 88 sessions), respectively. Functional sensory mapping confirmed that locations and response amplitudes of primary somatosensory subareas were not markedly different between Emx1G6$_{15q\ dup}$ mice and Emx1G6 mice (Figure S6), although the area responsive to whisker stimuli was larger in Emx1G6$_{15q\ dup}$ mice (Figures S6C and S6D), as reported in our previous study.[20]

Although the fluorescence changes at locomotion onset and cessation in Emx1G6$_{15q\ dup}$ mice were generally similar to those in Emx1G6 mice (Figure 6D, see also Figure 2A), the magnitude of changes in a few areas, such as PTa (mean ± SD; Emx1G6$_{15q\ dup}$, −0.10% ± 0.21%; Emx1G6, 1.33% ± 0.29% at 0 s) and BCm (Emx1G6$_{15q\ dup}$, −0.15% ± 0.20%; Emx1G6, 0.63% ± 0.15% at 0 s), were low (Figure 6D). These differences were not likely due to different baseline fluorescence

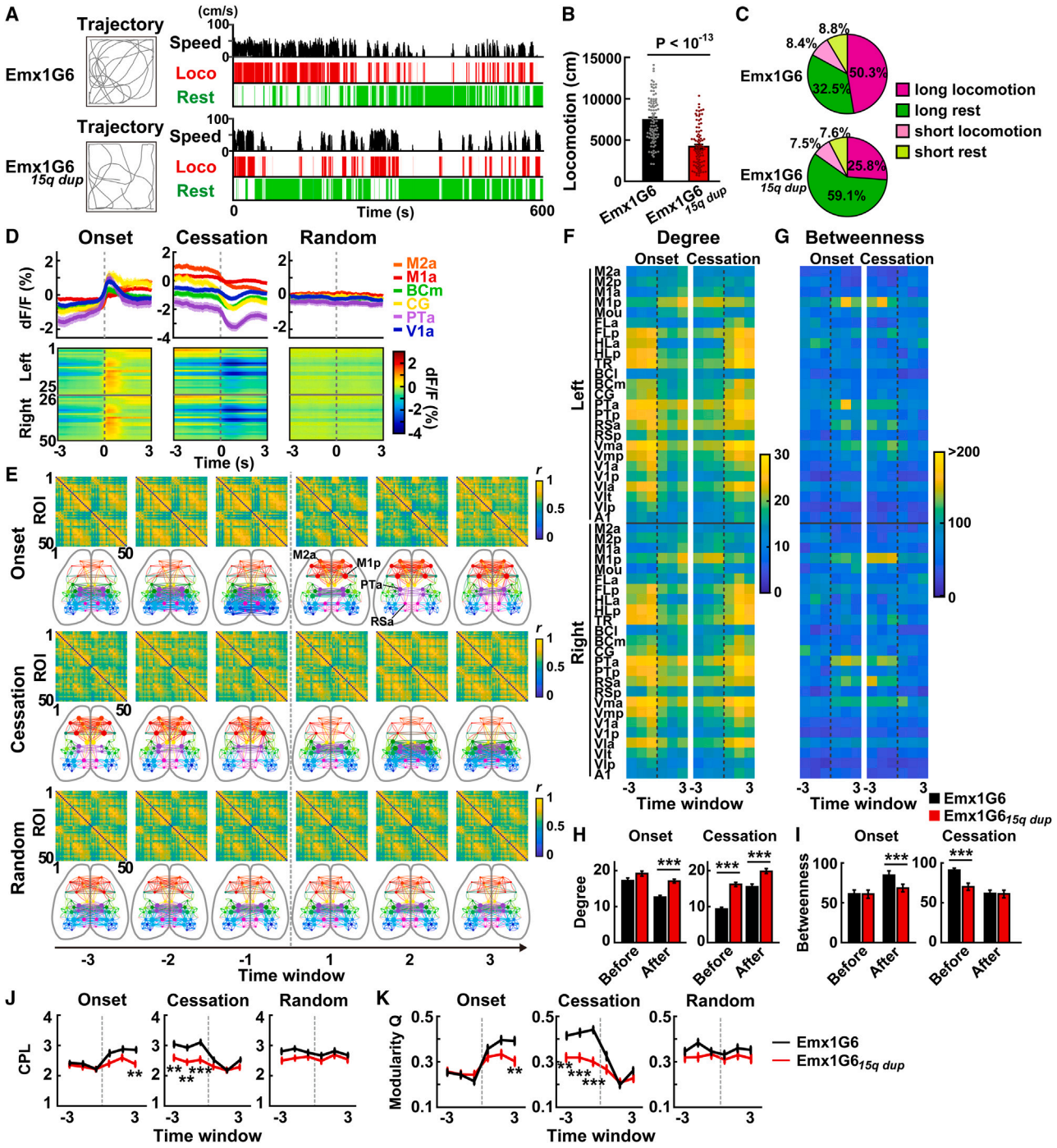

Figure 6. Hyperconnectivity and lower modularity of functional cortical networks in Emx1G6$_{15q\ dup}$ mice during behavioral state transitions

(A) Representative trajectory (left) and locomotion behavior (right) for Emx1G6 mice and Emx1G6$_{15q\ dup}$ mice. Locomotion speed and periods of locomotion (Loco) and rest of each genotype are shown from top to bottom in the right panel.

(B) Locomotor activity of Emx1G6 mice and Emx1G6$_{15q\ dup}$ mice during 10-min sessions. Data represent mean ± SEM; p value by t test. n = 89 sessions from seven Emx1G6 mice and 88 sessions from nine Emx1G6$_{15q\ dup}$ mice.

(C) Percentages of time spent for each type of episode in Emx1G6 mice and Emx1G6$_{15q\ dup}$ mice. Data represent averages across all sessions.

(D) Cortical activity of Emx1G6$_{15q\ dup}$ mice during the behavioral transitions. The convention of the figure is the same as in Figure 2A.

(E) Dynamics of correlations between activities of ROI pairs during the transitions in Emx1G6$_{15q\ dup}$ mice. FC graphs ($r > 0.8$) were generated using the data shown in (D). The convention of the figure is the same as in Figure 2B.

(F and G) Changes in node degree (F) and betweenness centrality (G) during the transitions in each ROI of Emx1G6$_{15q\ dup}$ mice.

(legend continued on next page)

levels in Emx1G6$_{15q\ dup}$ mice, as average fluorescence intensities of each cortical area were only slightly higher in these mice (Figure S6E). The overall patterns of FC networks in Emx1G6$_{15q\ dup}$ mice were also similar to those in Emx1G6 mice (Figure 6E, see also Figure 2B). However, the strength of FC appeared higher in Emx1G6$_{15q\ dup}$ mice, particularly FCs connecting ROIs in anterolateral motor cortices (i.e., M1 and M2) and FCs bridging anterior and posterior cortex (e.g., M1, PT, and RS) during locomotion (Figure 6E), as supported by generally larger node degrees compared with Emx1G6 mice (Figures 6F and 6H). In Emx1G6$_{15q\ dup}$ mice, betweenness centrality, CPL, and modularity Q were significantly lower than in Emx1G6 mice during locomotion (Figures 6I–6K), suggesting that cortical hyperconnectivity results in a less modularized, more interconnected network in behaving Emx1G6$_{15q\ dup}$ mice. Given the baseline hyperconnectivity in Emx1G6$_{15q\ dup}$ mice, surprisingly fewer locomotion-dependent decorrelations were detected, particularly in the posterior cortex (Figure S7). These findings collectively demonstrate that functional cortical networks in Emx1G6$_{15q\ dup}$ mice exhibit hyperconnectivity and enhanced interconnectivity, but a locomotion-related reconfiguration of network architecture is dampened compared with Emx1G6 mice.

Diagnosis of ASD model mice using temporal FC during behavioral transitions

Compared with Emx1G6 mice, we found that Emx1G6$_{15q\ dup}$ mice were characterized by significant hyperconnectivity of M2 and M1 areas during the transitions, most notably 1 s after onset and 2 s after cessation of movement (Figures 7A and 7B). The connections of M2 were right hemisphere dominant, while those of M1 appeared left hemisphere dominant (Figure S8D). Bilateral connections of somatosensory nodes (especially HL and TR) were significantly decorrelated compared with Emx1G6 mice regardless of behavioral state (Figures 7A and 7B). In addition, FCs between right PT and left M1, M2, FL, and HL showed decorrelation during locomotion, most evidently before cessation (Figures 7B and S8D).

To identify FC features that most distinguished Emx1G6$_{15q\ dup}$ mice from Emx1G6 mice, we conducted SVM classification of FC during locomotion onset and cessation into the two genotypes. The SVM classifiers trained with all features (All FCs) at each time point during behavior transitions accurately classified the Emx1G6$_{15q\ dup}$ and Emx1G6 genotypes (Figures 7C–7F). As with behavior state classification, the SVM classifiers trained with top 0.5% and bottom 0.5% features (Top + Bottom) performed comparably with the classifiers trained with all FCs, and significantly more accurately classified FC than the classifiers trained with randomly selected 1% features (Random) at all time points (Figures 7C and 7D). FCs including M2 and M1 were significantly over-represented in the top 0.5% and bottom 0.5% of features (Figures 7E and 7F), pointing to these cortical areas as key nodes that primarily contribute to deficits of cortical processing during spontaneous behavioral switching of Emx1G6$_{15q\ dup}$ mice.

Finally, we tested the importance of the behavior transition periods for genotype classification. The accuracies of classifiers trained with data from the locomotion that occurred within the transition periods (median accuracy, After-On, 100%; Before-Ces, 100%; Figure 7G) were significantly higher than those trained with data from continuous locomotion outside the transition (Out, 56.3%; Figure 7G). Similarly, classifiers trained with datasets from the rest that occurred within the transition periods more accurately classified FC into the correct genotype than classifiers trained with the data from continuous rest periods outside the transition (Before-On, 92.9%; After-Ces, 100%; Out, 84.5%; Figure 7H). In summary, these results demonstrate that the distinguishability of FC is greater during transition periods than during continuous locomotion and rest.

DISCUSSION

In this study, we investigated locomotion-induced changes in rapid cortico-cortical FC on the timescale of seconds by taking advantage of an integrated platform for mesoscopic Ca^{2+} imaging and VR that allows mice to run spontaneously with sensory feedback. Neural activity signals obtained using fluorescent Ca^{2+} indicator proteins are faster and typically more spatially resolved than BOLD signals. FC measured using fMRI and mesoscopic functional imaging is shown to overlap mainly with underlying structural connectivity[24–26] and reflect the correlation of modulation of neuronal spiking and local field potential (LFP) power between brain regions.[27–29] Our correlation-based FC analysis thus highlighted communication and interaction between cortical areas based on the level of local activity.

Cortical FC dynamics during behavioral transitions with and without visual information

The locomotion-dependent cortical functional network changes revealed in this study align with previous observations.[27,30–34] Recent imaging studies demonstrate that M2, which has dense reciprocal anatomic connections with sensory, parietal, and retrosplenial cortices,[35] orchestrates widespread cortical activity

(H and I) Mean node degree (H) and mean betweenness centrality (I) during the transitions. Data across all ROIs were averaged. ***$p < 0.001$, t test, n = 89 sessions from seven Emx1G6 mice and 88 sessions from nine Emx1G6$_{15q\ dup}$ mice.
(J and K) Change in CPL (J) and modularity Q (K) during the transitions in Emx1G6$_{15q\ dup}$ mice. The data for Emx1G6 mice presented in Figure 2 are again shown in black for comparison. Data represent mean ± SEM. (CPL) Onset, time, $F_{(5,\ 1014)} = 10.35$, $p = 1.1 \times 10^{-9}$; genotype, $F_{(1,\ 1014)} = 19.09$, $p = 1.4 \times 10^{-5}$; time × genotype, $F_{(5,\ 1014)} = 2.30$, $p = 0.04$; cessation, time, $F_{(5,\ 1026)} = 19.60$, $p = 1.1 \times 10^{-18}$; genotype, $F_{(1,\ 1026)} = 47.70$, $p = 8.7 \times 10^{-12}$; time × genotype, $F_{(5,\ 1026)} = 3.37$, $p = 0.005$; random, time, $F_{(5,\ 1050)} = 1.28$, $p = 0.27$; genotype, $F_{(1,\ 1050)} = 16.18$, $p = 6.2 \times 10^{-5}$; time × genotype, $F_{(5,\ 1050)} = 0.49$, $p = 0.78$; (modularity Q) onset, time, $F_{(5,\ 1014)} = 25.25$, $p = 4.7 \times 10^{-24}$; genotype, $F_{(1,\ 1014)} = 6.73$, $p = 0.01$; time × genotype, $F_{(5,\ 1014)} = 3.53$, $p = 0.004$; cessation, time, $F_{(5,\ 1026)} = 38.98$, $p = 1.0 \times 10^{-36}$; genotype, $F_{(1,\ 1026)} = 53.33$, $p = 5.6 \times 10^{-13}$; time × genotype, $F_{(5,\ 1026)} = 5.49$, $p = 5.4 \times 10^{-5}$; random, time, $F_{(5,\ 1050)} = 0.82$, $p = 0.54$; genotype, $F_{(1,\ 1050)} = 10.23$, $p = 0.001$; time × genotype, $F_{(5,\ 1050)} = 0.52$, $p = 0.76$, two-way ANOVA. **$p < 0.01$, ***$p < 0.001$ vs. Emx1G6, Tukey-Kramer test. n = 89 sessions from seven Emx1G6 mice and 88 sessions from nine Emx1G6$_{15q\ dup}$ mice.
See also Figures S6–S8.

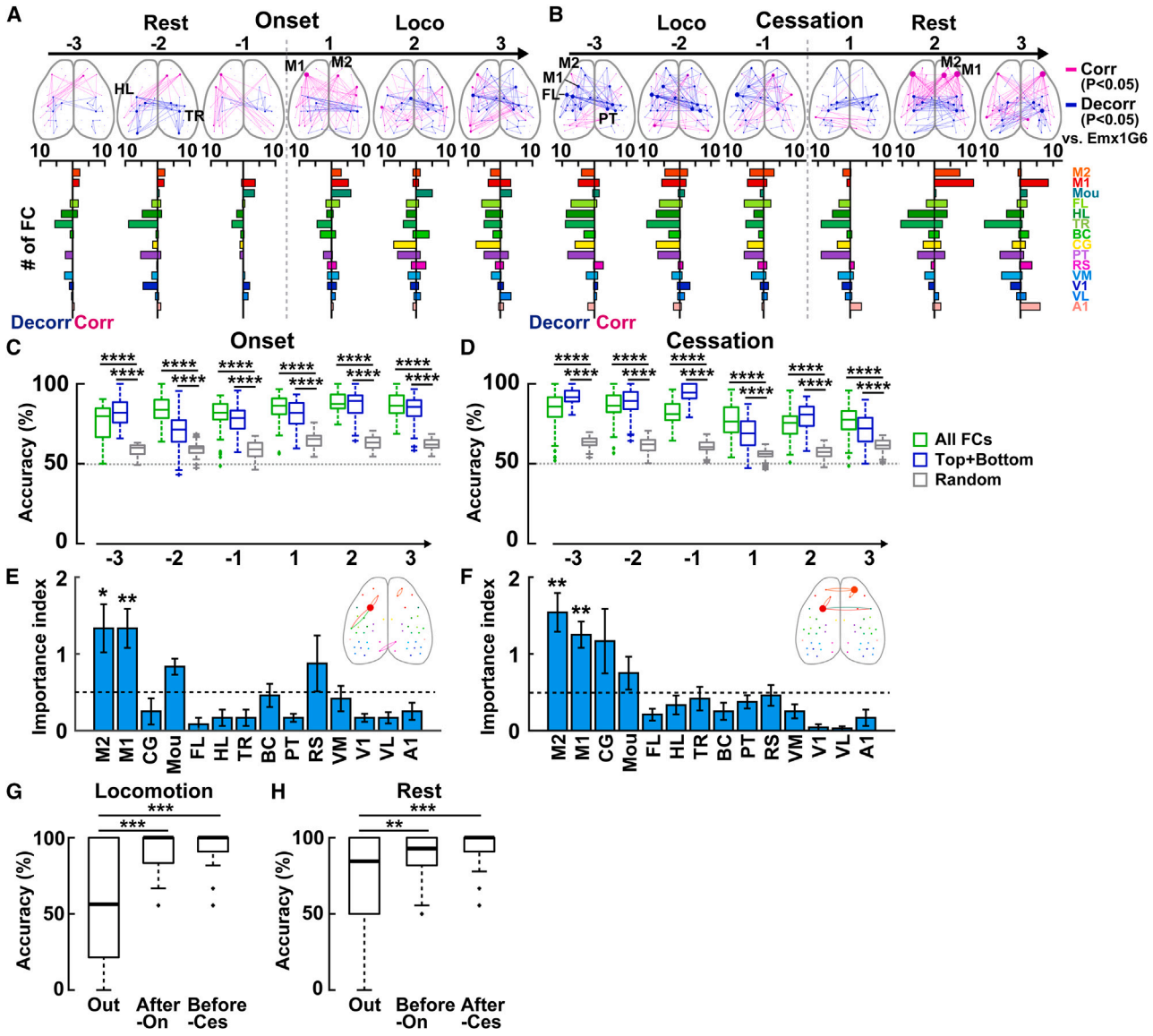

Figure 7. Importance of motor areas and behavioral transitions in distinguishing cortical FC between Emx1G6$_{15q\ dup}$ and Emx1G6 mice

(A and B) Statistically significant FC of Emx1G6$_{15q\ dup}$ mice during locomotion onset (A) and cessation (B) compared with Emx1G6 mice. The convention of the figure is the same as in Figure 4A. $p < 0.05$, NBS. n = 89 sessions from seven Emx1G6 mice and 88 sessions from nine Emx1G6$_{15q\ dup}$ mice.

(C and D) Accuracy of SVM classification of FC into two genotypes during locomotion onset (C) and cessation (D). Classifiers were trained with all 1,225 features (all FCs), top 0.5% and bottom 0.5% features (Top+Bottom), or randomly chosen 1% features (Random) at each time point. Only the periods of behavior transitions were considered in this classification. The boxes represent the 25th, 50th, and 75th percentiles, and the whiskers represent the range except for outliers. ****$p < 0.0001$ vs. Random, Wilcoxon rank-sum test with Bonferroni correction. n = 63 classifiers each.

(E and F) The importance index of each cortical area in the SVM classification of FC during locomotion onset (E) and cessation (F) was averaged across all relevant time points. Data represent mean ± SEM (n = 6 time points). The dashed line indicates a chance level defined as an average of 100-times random sampling of 1% features. (Inset) FCs that appeared frequently in the top 0.5% and bottom 0.5% features (>50% of total six time points, each of which was an average of 63 classifiers). *$p < 0.05$, **$p < 0.01$ vs. chance level, Wilcoxon rank-sum test with Bonferroni correction.

(G and H) Accuracy of SVM genotype classifiers trained with FC during locomotion (G) and rest (H) with or without transitions. The periods of locomotion were subdivided into those that occurred immediately after locomotion onset (After-On), immediately before locomotion cessation (Before-Ces), and any locomotion periods excluding SL that were outside these two types of periods (Out). Similarly, the periods of rest were subdivided into those that occurred immediately before locomotion onset (Before-On), immediately after locomotion cessation (After-Ces), and any rest periods excluding SR that were outside these two types of periods (Out). **$p < 0.01$, ***$p < 0.001$ vs. Out, Wilcoxon rank-sum test with Bonferroni correction. n = 63 classifiers each.

See also Figure S8.

during motor learning and decision-making tasks.[30,33] In our study, in line with the view that M2 acts to link antecedent conditions such as sensory information to motor actions,[36] M2 showed a transient elevation of significant correlation with multiple sensory areas at 1–2 s ahead of locomotion onset, regardless of the presence or absence of visual information (Figures 4A and 4C). Recently, a study that investigated cortical FC dynamics during locomotion also highlighted the importance of M2.[34] However, the role of sensory information for FC in this node had not been directly examined. Here, we found that FC between M2 and sensory cortices, including primary somatosensory cortex (S1) and primary visual cortex (V1), was decorrelated at 1 s after locomotion onset and demonstrated that this decorrelation completely disappeared when visual information was not available (Figures 4A and 4C). Although the elucidation of the underlying neural mechanisms requires further investigation, this may be relevant to the reported findings that locomotion with visual feedback drives V1 more strongly than without feedback and that direct top-down input from M2 to V1 sends motor-related signals for visual flow predictions.[31,32]

The FC associated with S1 significantly contributed to the SVM classification of locomotion and rest (Figure 5C). Remarkably, a dense correlated network among nodes of sensory areas, including S1, exhibited widespread and gradual augmentation over a period of 2 s before locomotion onset, but this characteristic functional subnetwork was no longer evident once locomotion started (Figure 4A). This preparatory emergence of a correlated network is reminiscent of the synchronous oscillations observed in S1 during premovement attentive immobility[37,38] and might also be relevant to the recent finding that S1 neuronal activity is highly correlated with the onset of movement.[39] Our analysis of fast FC dynamics was thus able to capture a global picture of distributed transient functional subnetworks that may play a role in the preparation and initiation of voluntary movement.

Cortical FC abnormalities in *15q dup* mice

Our FC analysis of a mouse model of ASD uncovered previously unknown impairment of cortical circuit function such as widespread hyperconnectivity, less modularized network during locomotion, and FC patterns involving M2 and M1 as the most distinctive signature for *15q dup* mice.

It has been reported that individuals with ASD exhibit motor coordination deficits and impairment of movement planning in goal-directed locomotion.[10–12] Although various factors could influence the locomotor activity of mice, reduced time spent for long locomotion in Emx1G6$_{15q\ dup}$ mice might result from impaired motor planning and execution due to abnormal M2-related FC. While human Dup15q syndrome shows a gait pattern of the slow pace, poor postural control, and large gait variability,[40] and patients with paternal duplication in 15q11-13 display clumsy motor skill development,[41] *15q dup* mice were also reported to display mild motor impairment such as longer stride length and reduced stride frequency, and deficits in motor learning and cerebellar synaptic plasticity.[42] Since recent studies demonstrate that cerebellar output modulates preparatory activity in the anterolateral motor cortex,[43,44] the abnormal M2-related FC we observed during behavior state transitions may also arise as a consequence of deficiency of a more widespread functional network, potentially including interactions with extracortical brain regions.

Compared with Emx1G6 mice, Emx1G6$_{15q\ dup}$ mice show significant decorrelation of FC that links M2, CG, S1, and PT during locomotion (Figures 7A and 7B). This subnetwork is reminiscent of the human lateral frontoparietal network (L-FPN), which consists of the rostral and dorsolateral prefrontal cortex and the inferior parietal cortex and participates in executive functions such as goal-directed cognition and task switching.[45] In task-based fMRI studies, atypical activation of L-FPN is observed during cognitive flexibility tasks in ASD brains.[46] Thus, it would be of interest in the future to investigate whether abnormal interaction between nodes of a mouse L-FPN equivalent in *15 dup* mice is implicated in impaired behavioral flexibility observed in reversed learning tests of the Morris water maze and Barnes maze.[18]

Future outlook

Our machine learning classification results demonstrate that information regarding an animal's ongoing behavioral state is represented in the fast dynamics of global cortical FC patterns (Figure 5). Identification of brain activity-based ASD biomarkers and machine learning-assisted diagnosis of ASD using neuroimaging data are fields of active investigation.[8,9,47] While recent human fMRI studies have begun to explore the use of dynamic resting-state FC to identify atypical brain network activity unique to ASD,[46,47] our results highlight the importance of examining behavioral transitions rather than simply looking at the resting state (Figures 7C–7H). Exploring additional mouse models will accumulate more evidence to identify common FC changes beyond the heterogeneity of ASD.[48] Furthermore, in future studies, it is of great interest to investigate whether the observed FC abnormalities can be reversed by pharmacologic treatment during postnatal development or adulthood of ASD model mice. Particularly, since postnatal chronic selective serotonin reuptake inhibitor (SSRI) treatment restores cortical excitatory-inhibitory balance and sensory tuning impaired in *15q dup* mice,[20] serotonergic interventions may also correct abnormal cortical FCs and the relevant behaviors.

Thus, our system to examine locomotion-dependent rapid FC changes based on mesoscopic cortex-wide Ca^{2+} imaging and VR offers a new translational approach toward developing precise diagnostic tools and effective treatment for various brain disorders. A fascinating future possibility would be to create a multimodal "metaverse" in which mice interact with other conspecifics via their avatars to understand cortical FC dynamics during virtual social interaction.[49]

Limitations of the study

Unlike awake fMRI,[5] our mesoscopic Ca^{2+} imaging only visualized the activity of the dorsal cortex, and the FC that involved the ventral cortex and other subcortical areas could not be examined in this study. In addition, neural activity signals we monitored likely came from layer 1 and layer 2/3, which contained cell bodies and dendrites of local pyramidal neurons and superficial axons innervating them, although the signals as a whole most likely reflect local cortical activity.[33] Improved and newly emerging technologies will help advance future studies toward a more precise and comprehensive illustration of fast FC dynamics across the whole brain.[50,51]

STAR★METHODS

Detailed methods are provided in the online version of this paper and include the following:

- KEY RESOURCES TABLE
- RESOURCE AVAILABILITY
  - Lead contact
  - Materials availability
  - Data and code availability
- EXPERIMENTAL MODEL AND SUBJECT DETAILS
  - Mice
- METHOD DETAILS
  - Surgery
  - VR environment
  - Behavioral testing and mesoscopic cortical-wide Ca^{2+} imaging
  - Histology
- QUANTIFICATION AND STATISTICAL ANALYSIS
  - ROI selection
  - Data analysis
  - Support vector machine classification
  - Statistics

SUPPLEMENTAL INFORMATION

Supplemental information can be found online at https://doi.org/10.1016/j.celrep.2023.112258.

ACKNOWLEDGMENTS

We thank Norihiro Sadato, Masaki Fukunaga, and Takahiko Koike for their advice on the network analyses, Yasunori Hayashi for general support, and Hiromu Monai for comments on this manuscript. This work was supported by KAKENHI from JSPS, 19H04942 (N.N.), 17H05985, 19H04942, and 20H03550 (M.S.), and 16H06316, 16H06463, 16H06276, 21H00202, 21H04813, and 21K19351 (T.T.); The Incentive Research Project grant from RIKEN (N.N.); Taiju Life Social Welfare Foundation (M.S. and T.T.); Japan Agency for Medical Research and Development, JP21wm0425011; Japan Science and Technology Agency, JPMJMS2299, JPMJMS229B; Intramural Research Grant (30-9) for Neurological and Psychiatric Disorders of NCNP; The Takeda Science Foundation; Smoking Research Foundation; Tokyo Biochemical Research Foundation; Research Foundation for Opto-Science and Technology; The Naito Foundation; and The Tokumori Yasumoto Memorial Trust for Researches on Tuberous Sclerosis Complex and Related Rare Neurological Diseases (T.T.).

AUTHOR CONTRIBUTIONS

Conceptualization, N.N.; methodology, N.N., M.S., and O.Y.; investigation, N.N., Y.S., and X.F.; visualization, N.N.; writing – original draft, N.N.; writing – review & editing, N.N., M.S., O.Y., A.Z., and T.T.; funding acquisition, N.N., M.S., and T.T.; supervision, M.S., J.N., and T.T.

DECLARATION OF INTERESTS

The authors declare no competing interests.

INCLUSION AND DIVERSITY

We support inclusive, diverse, and equitable conduct of research.

Received: September 9, 2022
Revised: February 16, 2023
Accepted: February 28, 2023
Published: March 28, 2023

REFERENCES

1. Ferezou, I., Haiss, F., Gentet, L.J., Aronoff, R., Weber, B., and Petersen, C.C.H. (2007). Spatiotemporal dynamics of cortical sensorimotor integration in behaving mice. Neuron *56*, 907–923. https://doi.org/10.1016/j.neuron.2007.10.007.
2. van den Heuvel, M.P., and Hulshoff Pol, H.E. (2010). Exploring the brain network: a review on resting-state fMRI functional connectivity. Eur. Neuropsychopharmacol. *20*, 519–534. https://doi.org/10.1016/j.euroneuro.2010.03.008.
3. Honey, C.J., Kötter, R., Breakspear, M., and Sporns, O. (2007). Network structure of cerebral cortex shapes functional connectivity on multiple time scales. Proc. Natl. Acad. Sci. USA *104*, 10240–10245. https://doi.org/10.1073/pnas.0701519104.
4. Gozzi, A., and Schwarz, A.J. (2016). Large-scale functional connectivity networks in the rodent brain. Neuroimage *127*, 496–509. https://doi.org/10.1016/j.neuroimage.2015.12.017.
5. Tsurugizawa, T., Tamada, K., Ono, N., Karakawa, S., Kodama, Y., Debacker, C., Hata, J., Okano, H., Kitamura, A., Zalesky, A., and Takumi, T. (2020). Awake functional MRI detects neural circuit dysfunction in a mouse model of autism. Sci. Adv. *6*, eaav4520. https://doi.org/10.1126/sciadv.aav4520.
6. Minshew, N.J., and Keller, T.A. (2010). The nature of brain dysfunction in autism: functional brain imaging studies. Curr. Opin. Neurol. *23*, 124–130. https://doi.org/10.1097/WCO.0b013e32833782d4.
7. Hull, J.V., Dokovna, L.B., Jacokes, Z.J., Torgerson, C.M., Irimia, A., and Van Horn, J.D. (2016). Resting-state functional connectivity in autism spectrum disorders: a review. Front. Psychiatry *7*, 205. https://doi.org/10.3389/fpsyt.2016.00205.
8. Eslami, T., Almuqhim, F., Raiker, J.S., and Saeed, F. (2020). Machine learning methods for diagnosing autism spectrum disorder and attention-deficit/hyperactivity disorder using functional and structural MRI: a survey. Front. Neuroinform. *14*, 575999. https://doi.org/10.3389/fninf.2020.575999.
9. Uddin, L.Q., Dajani, D.R., Voorhies, W., Bednarz, H., and Kana, R.K. (2017). Progress and roadblocks in the search for brain-based biomarkers of autism and attention-deficit/hyperactivity disorder. Transl. Psychiatry *7*, e1218. https://doi.org/10.1038/tp.2017.164.
10. Fournier, K.A., Hass, C.J., Naik, S.K., Lodha, N., and Cauraugh, J.H. (2010). Motor coordination in autism spectrum disorders: a synthesis and meta-analysis. J. Autism Dev. Disord. *40*, 1227–1240. https://doi.org/10.1007/s10803-010-0981-3.
11. Longuet, S., Ferrel-Chapus, C., Orève, M.J., Chamot, J.-M., and Vernazza-Martin, S. (2012). Emotion, intent and voluntary movement in children with autism. An example: the goal directed locomotion. J. Autism Dev. Disord. *42*, 1446–1458. https://doi.org/10.1007/s10803-011-1383-x.
12. Vernazza-Martin, S., Martin, N., Vernazza, A., Lepellec-Muller, A., Rufo, M., Massion, J., and Assaiante, C. (2005). Goal directed locomotion and balance control in autistic children. J. Autism Dev. Disord. *35*, 91–102. https://doi.org/10.1007/s10803-004-1037-3.
13. Hannant, P., Tavassoli, T., and Cassidy, S. (2016). The role of sensorimotor difficulties in autism spectrum conditions. Front. Neurol. *7*, 124. https://doi.org/10.3389/fneur.2016.00124.
14. Cardin, J.A., Crair, M.C., and Higley, M.J. (2020). Mesoscopic imaging: shining a wide light on large-scale neural dynamics. Neuron *108*, 33–43. https://doi.org/10.1016/j.neuron.2020.09.031.
15. Ren, C., and Komiyama, T. (2021). Characterizing cortex-wide dynamics with wide-field calcium imaging. J. Neurosci. *41*, 4160–4168. https://doi.org/10.1523/JNEUROSCI.3003-20.2021.

16. Sato, M., Kawano, M., Mizuta, K., Islam, T., Lee, M.G., and Hayashi, Y. (2017). Hippocampus-dependent goal localization by head-fixed mice in virtual reality. eNeuro *4*, ENEURO.0369–16.2017. https://doi.org/10.1523/ENEURO.0369-16.2017.

17. Sato, M., Mizuta, K., Islam, T., Kawano, M., Sekine, Y., Takekawa, T., Gomez-Dominguez, D., Schmidt, A., Wolf, F., Kim, K., et al. (2020). Distinct mechanisms of over-representation of landmarks and rewards in the Hippocampus. Cell Rep. *32*, 107864. https://doi.org/10.1016/j.celrep.2020.107864.

18. Nakatani, J., Tamada, K., Hatanaka, F., Ise, S., Ohta, H., Inoue, K., Tomonaga, S., Watanabe, Y., Chung, Y.J., Banerjee, R., et al. (2009). Abnormal behavior in a chromosome-engineered mouse model for human 15q11-13 duplication seen in autism. Cell *137*, 1235–1246. https://doi.org/10.1016/j.cell.2009.04.024.

19. Tamada, K., Fukumoto, K., Toya, T., Nakai, N., Awasthi, J.R., Tanaka, S., Okabe, S., Spitz, F., Saitow, F., Suzuki, H., and Takumi, T. (2021). Genetic dissection identifies Necdin as a driver gene in a mouse model of paternal 15q duplications. Nat. Commun. *12*, 4056. https://doi.org/10.1038/s41467-021-24359-3.

20. Nakai, N., Nagano, M., Saitow, F., Watanabe, Y., Kawamura, Y., Kawamoto, A., Tamada, K., Mizuma, H., Onoe, H., Watanabe, Y., et al. (2017). Serotonin rebalances cortical tuning and behavior linked to autism symptoms in 15q11-13 CNV mice. Sci. Adv. *3*, e1603001. https://doi.org/10.1126/sciadv.1603001.

21. Rubinov, M., and Sporns, O. (2010). Complex network measures of brain connectivity: uses and interpretations. Neuroimage *52*, 1059–1069. https://doi.org/10.1016/j.neuroimage.2009.10.003.

22. Harris, K.D., and Thiele, A. (2011). Cortical state and attention. Nat. Rev. Neurosci. *12*, 509–523. https://doi.org/10.1038/nrn3084.

23. Zalesky, A., Fornito, A., and Bullmore, E.T. (2010). Network-based statistic: identifying differences in brain networks. Neuroimage *53*, 1197–1207. https://doi.org/10.1016/j.neuroimage.2010.06.041.

24. Damoiseaux, J.S., and Greicius, M.D. (2009). Greater than the sum of its parts: a review of studies combining structural connectivity and resting-state functional connectivity. Brain Struct. Funct. *213*, 525–533. https://doi.org/10.1007/s00429-009-0208-6.

25. Koch, M.A., Norris, D.G., and Hund-Georgiadis, M. (2002). An investigation of functional and anatomical connectivity using magnetic resonance imaging. Neuroimage *16*, 241–250. https://doi.org/10.1006/nimg.2001.1052.

26. Mohajerani, M.H., Chan, A.W., Mohsenvand, M., LeDue, J., Liu, R., McVea, D.A., Boyd, J.D., Wang, Y.T., Reimers, M., and Murphy, T.H. (2013). Spontaneous cortical activity alternates between motifs defined by regional axonal projections. Nat. Neurosci. *16*, 1426–1435. https://doi.org/10.1038/nn.3499.

27. Clancy, K.B., Orsolic, I., and Mrsic-Flogel, T.D. (2019). Locomotion-dependent remapping of distributed cortical networks. Nat. Neurosci. *22*, 778–786. https://doi.org/10.1038/s41593-019-0357-8.

28. Nir, Y., Mukamel, R., Dinstein, I., Privman, E., Harel, M., Fisch, L., Gelbard-Sagiv, H., Kipervasser, S., Andelman, F., Neufeld, M.Y., et al. (2008). Interhemispheric correlations of slow spontaneous neuronal fluctuations revealed in human sensory cortex. Nat. Neurosci. *11*, 1100–1108. https://doi.org/10.1038/nn.2177.

29. Shmuel, A., and Leopold, D.A. (2008). Neuronal correlates of spontaneous fluctuations in fMRI signals in monkey visual cortex: implications for functional connectivity at rest. Hum. Brain Mapp. *29*, 751–761. https://doi.org/10.1002/hbm.20580.

30. Allen, W.E., Kauvar, I.V., Chen, M.Z., Richman, E.B., Yang, S.J., Chan, K., Gradinaru, V., Deverman, B.E., Luo, L., and Deisseroth, K. (2017). Global representations of goal-directed behavior in distinct cell types of mouse neocortex. Neuron *94*, 891–907.e6. https://doi.org/10.1016/j.neuron.2017.04.017.

31. Keller, G.B., Bonhoeffer, T., and Hübener, M. (2012). Sensorimotor mismatch signals in primary visual cortex of the behaving mouse. Neuron *74*, 809–815. https://doi.org/10.1016/j.neuron.2012.03.040.

32. Leinweber, M., Ward, D.R., Sobczak, J.M., Attinger, A., and Keller, G.B. (2017). A sensorimotor circuit in mouse cortex for visual flow predictions. Neuron *95*, 1420–1432.e5. https://doi.org/10.1016/j.neuron.2017.08.036.

33. Makino, H., Ren, C., Liu, H., Kim, A.N., Kondapaneni, N., Liu, X., Kuzum, D., and Komiyama, T. (2017). Transformation of cortex-wide emergent properties during motor learning. Neuron *94*, 880–890.e8. https://doi.org/10.1016/j.neuron.2017.04.015.

34. West, S.L., Aronson, J.D., Popa, L.S., Feller, K.D., Carter, R.E., Chiesl, W.M., Gerhart, M.L., Shekhar, A.C., Ghanbari, L., Kodandaramaiah, S.B., and Ebner, T.J. (2022). Wide-field calcium imaging of dynamic cortical networks during locomotion. Cereb. Cortex *32*, 2668–2687. https://doi.org/10.1093/cercor/bhab373.

35. Zingg, B., Hintiryan, H., Gou, L., Song, M.Y., Bay, M., Bienkowski, M.S., Foster, N.N., Yamashita, S., Bowman, I., Toga, A.W., and Dong, H.W. (2014). Neural networks of the mouse neocortex. Cell *156*, 1096–1111. https://doi.org/10.1016/j.cell.2014.02.023.

36. Barthas, F., and Kwan, A.C. (2017). Secondary motor cortex: where "sensory" meets "motor" in the rodent frontal cortex. Trends Neurosci. *40*, 181–193. https://doi.org/10.1016/j.tins.2016.11.006.

37. Mackay, W.A. (1997). Synchronized neuronal oscillations and their role in motor processes. Trends Cogn. Sci. *1*, 176–183. https://doi.org/10.1016/S1364-6613(97)01059-0.

38. Nicolelis, M.A., Baccala, L.A., Lin, R.C., and Chapin, J.K. (1995). Sensorimotor encoding by synchronous neural ensemble activity at multiple levels of the somatosensory system. Science *268*, 1353–1358. https://doi.org/10.1126/science.7761855.

39. Karadimas, S.K., Satkunendrarajah, K., Laliberte, A.M., Ringuette, D., Weisspapir, I., Li, L., Gosgnach, S., and Fehlings, M.G. (2020). Sensory cortical control of movement. Nat. Neurosci. *23*, 75–84. https://doi.org/10.1038/s41593-019-0536-7.

40. Wilson, R.B., Elashoff, D., Gouelle, A., Smith, B.A., Wilson, A.M., Dickinson, A., Safari, T., Hyde, C., and Jeste, S.S. (2020). Quantitative gait analysis in duplication 15q syndrome and nonsyndromic ASD. Autism Res. *13*, 1102–1110. https://doi.org/10.1002/aur.2298.

41. Veltman, M.W.M., Thompson, R.J., Craig, E.E., Dennis, N.R., Roberts, S.E., Moore, V., Brown, J.A., and Bolton, P.F. (2005). A paternally inherited duplication in the Prader-Willi/Angelman syndrome critical region: a case and family study. J. Autism Dev. Disord. *35*, 117–127. https://doi.org/10.1007/s10803-004-1039-1.

42. Piochon, C., Kloth, A.D., Grasselli, G., Titley, H.K., Nakayama, H., Hashimoto, K., Wan, V., Simmons, D.H., Eissa, T., Nakatani, J., et al. (2014). Cerebellar plasticity and motor learning deficits in a copy-number variation mouse model of autism. Nat. Commun. *5*, 5586. https://doi.org/10.1038/ncomms6586.

43. Chabrol, F.P., Blot, A., and Mrsic-Flogel, T.D. (2019). Cerebellar contribution to preparatory activity in motor neocortex. Neuron *103*, 506–519.e4. https://doi.org/10.1016/j.neuron.2019.05.022.

44. Gao, Z., Davis, C., Thomas, A.M., Economo, M.N., Abrego, A.M., Svoboda, K., De Zeeuw, C.I., and Li, N. (2018). A cortico-cerebellar loop for motor planning. Nature *563*, 113–116. https://doi.org/10.1038/s41586-018-0633-x.

45. Uddin, L.Q., Yeo, B.T.T., and Spreng, R.N. (2019). Towards a universal taxonomy of macro-scale functional human brain networks. Brain Topogr. *32*, 926–942. https://doi.org/10.1007/s10548-019-00744-6.

46. Uddin, L.Q. (2021). Brain mechanisms supporting flexible cognition and behavior in adolescents with autism spectrum disorder. Biol. Psychiatry *89*, 172–183. https://doi.org/10.1016/j.biopsych.2020.05.010.

47. Du, Y., Fu, Z., and Calhoun, V.D. (2018). Classification and prediction of brain disorders using functional connectivity: promising but challenging. Front. Neurosci. *12*, 525. https://doi.org/10.3389/fnins.2018.00525.

48. Nakai, N., Takumi, T., Nakai, J., and Sato, M. (2018). Common defects of spine dynamics and circuit function in neurodevelopmental disorders: a systematic review of findings from in vivo optical imaging of mouse models. Front. Neurosci. *12*, 412. https://doi.org/10.3389/fnins.2018.00412.

49. Kingsbury, L., and Hong, W. (2020). A multi-brain framework for social interaction. Trends Neurosci. *43*, 651–666. https://doi.org/10.1016/j.tins.2020.06.008.

50. Gottschalk, S., Degtyaruk, O., Mc Larney, B., Rebling, J., Deán-Ben, X.L., Shoham, S., and Razansky, D. (2019). Isolated murine brain model for large-scale optoacoustic calcium imaging. Front. Neurosci. *13*, 290. https://doi.org/10.3389/fnins.2019.00290.

51. Shemesh, O.A., Linghu, C., Piatkevich, K.D., Goodwin, D., Celiker, O.T., Gritton, H.J., Romano, M.F., Gao, R., Yu, C.-C.J., Tseng, H.-A., et al. (2020). Precision calcium imaging of dense neural populations via a cell-body-targeted calcium indicator. Neuron *107*, 470–486.e11. https://doi.org/10.1016/j.neuron.2020.05.029.

52. Iwasato, T., Nomura, R., Ando, R., Ikeda, T., Tanaka, M., and Itohara, S. (2004). Dorsal telencephalon-specific expression of Cre recombinase in PAC transgenic mice. Genesis *38*, 130–138. https://doi.org/10.1002/gene.20009.

53. Steinmetz, N.A., Buetfering, C., Lecoq, J., Lee, C.R., Peters, A.J., Jacobs, E.A.K., Coen, P., Ollerenshaw, D.R., Valley, M.T., de Vries, S.E.J., et al. (2017). Aberrant cortical activity in multiple GCaMP6-expressing transgenic mouse lines. eNeuro *4*, ENEURO.0207–17.2017. https://doi.org/10.1523/ENEURO.0207-17.2017.

54. Cramer, J.V., Gesierich, B., Roth, S., Dichgans, M., Düring, M., and Liesz, A. (2019). In vivo widefield calcium imaging of the mouse cortex for analysis of network connectivity in health and brain disease. Neuroimage *199*, 570–584. https://doi.org/10.1016/j.neuroimage.2019.06.014.

55. Franklin, K., and Paxinos, G. (2003). The Mouse Brain in Stereotaxic Coordinates, Second Edition (Academic Press).

56. Kirkcaldie, M.T.K. (2012). Chapter 4 - neocortex. In The Mouse Nervous System, C. Watson, G. Paxinos, and L. Puelles, eds. (Academic Press), pp. 52–111. https://doi.org/10.1016/B978-0-12-369497-3.10004-4.

57. Tamada, K., Tomonaga, S., Hatanaka, F., Nakai, N., Takao, K., Miyakawa, T., Nakatani, J., and Takumi, T. (2010). Decreased exploratory activity in a mouse model of 15q duplication syndrome; implications for disturbance of serotonin signaling. PLoS One *5*, e15126. https://doi.org/10.1371/journal.pone.0015126.

58. Kozberg, M.G., Ma, Y., Shaik, M.A., Kim, S.H., and Hillman, E.M.C. (2016). Rapid postnatal expansion of neural networks occurs in an environment of altered neurovascular and neurometabolic coupling. J. Neurosci. *36*, 6704–6717. https://doi.org/10.1523/JNEUROSCI.2363-15.2016.

59. Shibuki, K., Hishida, R., Murakami, H., Kudoh, M., Kawaguchi, T., Watanabe, M., Watanabe, S., Kouuchi, T., and Tanaka, R. (2003). Dynamic imaging of somatosensory cortical activity in the rat visualized by flavoprotein autofluorescence. J. Physiol. *549*, 919–927. https://doi.org/10.1113/jphysiol.2003.040709.

60. Wekselblatt, J.B., Flister, E.D., Piscopo, D.M., and Niell, C.M. (2016). Large-scale imaging of cortical dynamics during sensory perception and behavior. J. Neurophysiol. *115*, 2852–2866. https://doi.org/10.1152/jn.01056.2015.

61. Gallero-Salas, Y., Han, S., Sych, Y., Voigt, F.F., Laurenczy, B., Gilad, A., and Helmchen, F. (2021). Sensory and behavioral components of neocortical signal flow in discrimination tasks with short-term memory. Neuron *109*, 135–148.e6. https://doi.org/10.1016/j.neuron.2020.10.017.

62. Gilad, A., and Helmchen, F. (2020). Spatiotemporal refinement of signal flow through association cortex during learning. Nat. Commun. *11*, 1744. https://doi.org/10.1038/s41467-020-15534-z.

63. Couto, J., Musall, S., Sun, X.R., Khanal, A., Gluf, S., Saxena, S., Kinsella, I., Abe, T., Cunningham, J.P., Paninski, L., and Churchland, A.K. (2021). Chronic, cortex-wide imaging of specific cell populations during behavior. Nat. Protoc. *16*, 3241–3263. https://doi.org/10.1038/s41596-021-00527-z.

64. MacDowell, C.J., and Buschman, T.J. (2020). Low-dimensional spatiotemporal dynamics underlie cortex-wide neural activity. Curr. Biol. *30*, 2665–2680.e8. https://doi.org/10.1016/j.cub.2020.04.090.

65. Stringer, C., Pachitariu, M., Steinmetz, N., Reddy, C.B., Carandini, M., and Harris, K.D. (2019). Spontaneous behaviors drive multidimensional, brain-wide activity. Science *364*, 255. https://doi.org/10.1126/science.aav7893.

66. Lim, D.H., LeDue, J.M., and Murphy, T.H. (2015). Network analysis of mesoscale optical recordings to assess regional, functional connectivity. Neurophotonics *2*, 041405. https://doi.org/10.1117/1.NPh.2.4.041405.

STAR★METHODS

KEY RESOURCES TABLE

REAGENT or RESOURCE	SOURCE	IDENTIFIER
Antibodies		
Rabbit anti-GFP antibody	Thermo Fisher Scientific	Cat# A-11122; RRID:AB_221569
Mouse anti-GAD67 antibody	Millipore	Cat# MAB5406; RRID:AB_2278725
Alexa 488-labeled goat anti-rabbit IgG antibody	Thermo Fisher Scientific	Cat# A-11034; RRID:AB_2576217
Alexa 568-labeled goat anti-mouse IgG antibody	Thermo Fisher Scientific	Cat# A-11019; RRID:AB_143162
Experimental models: Organisms/strains		
Mouse: C57BL6/J	Japan SLC	C57BL/6JJmsSlc
Mouse: Emx1-cre: B6.129P2-Emx1$^{tm1.1(cre)Ito}$/ItoRbrc	RIKEN BioResource Center	RRID:IMSR_RBRC01345
Mouse: Ai95D: B6;129S-Gt(ROSA)26Sor$^{tm95.1(CAG-GCaMP6f)Hze}$/J	The Jackson Laboratories	RRID:IMSR_JAX:024105
Mouse: *15q dup*: B6.129S7-Dp(7Herc2-Mkrn3)1Taku	RIKEN BioResource Center	RRID:IMSR_RBRC05954
Software and algorithms		
MATLAB	MathWorks	https://www.mathworks.com/
ImageJ	NIH	https://imagej.net/ij
LabVIEW	National Instruments	https://www.ni.com
Brain Connectivity Toolbox	Rubinov M. and Sporns O.[21]	https://sites.google.com/site/bctnet/
Network Based Statistics	Zalesky et al.[23]	https://www.nitrc.org/projects/nbs/
OmegaSpace	Solidray	https://www.solidray.co.jp/

RESOURCE AVAILABILITY

Lead contact

Further information and requests for resources and reagents should be directed to and will be fulfilled by the lead contact, Toru Takumi (takumit@med.kobe-u.ac.jp).

Materials availability

This study did not generate new unique reagents.

Data and code availability

All data reported in this paper will be shared by the lead contact upon request.
This paper does not report original code.
Any additional information required to reanalyze the data reported in this paper is available from the lead contact upon request.

EXPERIMENTAL MODEL AND SUBJECT DETAILS

Mice

The following Cre driver, reporter, and ASD model mouse lines were used for breeding; Emx1-cre (B6.129P2-Emx1$^{tm1.1(cre)Ito}$/ItoRbrc, RBRC01345, RIKEN Bioresource Center[52]), Ai95D (B6;129S-*Gt(ROSA)26Sor$^{tm95.1(CAG-GCaMP6f)Hze}$*/J, JAX024105, Jackson Laboratories), *15q dup* (B6.129S7-Dp(7Herc2-Mkrn3)1Taku, RBRC05954, RIKEN Bioresource Center[18]). Twenty-three Emx1G6 mice, nine Emx1G6$_{15q\ dup}$ mice, and three C57BL/6J (non-G6) mice (all male at 12–20 weeks old) were used for experiments. Although some genotypes of transgenic mice that express GCaMP6 reportedly exhibit cortical epileptiform fluorescence events (most often seen in Ai93 line),[53] we did not observe such aberrant activity in our combination of Emx1-cre mice and Ai95D mice. For experiments, Emx1G6 mice were obtained by crossing Emx1-cre mice with Ai95D mice. Emx1G6$_{15q\ dup}$ mice were obtained by crossing male mice double-positive for Emx1-Cre and *15q dup* and female mice positive for Ai95D. All mice were maintained

in a reverse 12 h dark/light cycle (light off at 8 a.m.), and experiments were conducted during the dark phase. Food and water were available *ad libitum*. All procedures were carried out following the institutional guidelines and protocols approved by the Institutional Animal Care and Use Committees of RIKEN and Kobe University.

METHOD DETAILS

Surgery

During surgery, mice were anesthetized under 1.5–2.0% isoflurane in air, and the body temperature was kept at 37°C using a heating pad. The scalp was cut off, and the surface of the skull was cleaned using a cotton swab. The skull surface was then covered with a thin layer of transparent resin (Super-Bond C&B, Sun Medical, Japan), followed by the placement of a coverslip (0.17 mm thickness, Matsunami, Japan) onto the resin layer.[54] A custom-made metal head plate with a polygonal imaging window (size of opening, 13 mm long and 10 mm wide, Narishige, Japan) was affixed to the edge of the coverslip with dental cement so that the entire dorsal cortex was clearly visible transcranially through the window (Figures 1C and 1G). The mice were allowed to fully recover from anesthesia in a warmed chamber and then returned to their home cages.

VR environment

A head-fixed mouse under microscopy was set on an air-floated spherical treadmill[16,17] (Figures 1A and 1B). The treadmill was composed of a 20-cm polystyrene foam ball and a hemispherical stainless steel bowl with an internal diameter that fitted with the ball. The bowl had eight holes for pressured air at the bottom. The head of the mouse was fixed to a rigid head mount bar and posts via the head plate and positioned ~1 cm above the top of the ball. The movement of mice was detected as rotations of the treadmill by two USB optical motion detectors (Gaming Mouse G302, Logicool) which were positioned orthogonal to each other on the equator of the treadmill. The movement signals from the motion detectors were transformed into analog output voltages using a custom-written LabVIEW program (National Instruments) to control the mouse's virtual position via a joystick controller (USB Joystick Interface, 909991, APEM) connected to the VR software (OmegaSpace ver 3.7, Solidray). An interactive VR landscape rendered from a first-person perspective was projected by two compact liquid crystal display (LCD) projectors (M110, Dell) onto the back of a custom-made 40 cm-diameter translucent acrylic semi-domal screen that was positioned 20 cm in front of the mouse and covered 240° of the mouse's visual field.

The VR landscape mimicked a realistic open-field enclosure and consisted of a two-dimensional square arena with different colored walls. When the mice hit the wall in the arena, they adhered to it visually, but no physical barrier prevented them from continuing their locomotion. They were therefore allowed to move until they spontaneously changed direction. Experiments without projection of VR landscape were conducted (5 sessions after final sessions in the normal condition) by turning off the LCD projectors (Figure 3).

Behavioral testing and mesoscopic cortical-wide Ca^{2+} imaging

Mice underwent three pre-training steps to acclimate to the test environment. In the first step, which began 3–5 days before surgery, mice were daily allowed to move freely on the top of the polystyrene foam ball that was rotated manually by an experimenter for 10 min and then handled by the experimenter under room light for another 10 min. The second step started as early as a day after surgery. In this step, mice were acclimated daily to head-fixation in the VR set-up for 3–5 days until they were able to sit and move on the treadmill in a balanced manner for 0.5–1 h under dim light (approximately 20 lux). In the final step, mice were acclimated to a complete VR environment and allowed to explore the virtual arena for 10 min daily for 5–10 days until they could move along the wall of the arena and turn the corner without difficulty.

After completing these pre-training processes, spontaneous locomotion within the virtual arena and cortical activity were recorded in a 10-min test session daily for a total of 15 sessions. The cortex was illuminated transcranially by a mercury lamp (U-HGLGPS, Olympus) through 460–480 nm (MGFPHQ, Olympus) or 457–487 nm (GFP-3035D, Semrock) excitation filters. Green fluorescence images were acquired using a CMOS camera (ORCA-Flash 4.0 v2, Hamamatsu) mounted on a HyperScope upright microscope (Scientifica) through a 2× objective lens (Plan Apo λ, NA: 0.10, Nikon) and 495–540 nm (Olympus) or 502.5–537.5 nm (Semrock) emission filters. Images of 512 × 512 pixels (14.8 μm × 14.8 μm/pixel; field of view, 7.5 mm × 7.5 mm) were collected at a rate of 30 frames per second while the head-fixed mouse freely explored the virtual arena. The mouse's locomotion speed and coordinates were recorded at a sampling rate of 60 Hz using custom LabVIEW software. The rising edge of the TTL (Transistor-transistor-logic) signals that the camera generated at the acquisition of each frame were detected and recorded simultaneously with the behavioral data for synchronization with the imaging data.

Histology

Mice were deeply anesthetized with isoflurane and perfused transcardially with phosphate-buffered saline (PBS), followed by 4% paraformaldehyde (PFA) in PBS. Brains were removed and further fixed in 4% PFA in PBS at 4°C overnight. Frozen parasagittal sections were cut on a cryostat to a thickness of 30 μm. The sections were incubated at 4°C overnight with rabbit anti-GFP antibody (1:1000, A-11122, Thermo Fisher Scientific) and mouse anti-GAD67 antibody (1:1000, MAB5406, Millipore) diluted in PBS containing 5% normal goat serum and 0.3% Triton X-100, followed by Alexa Fluor 488- or Alexa 568-labeled goat anti-rabbit or anti-mouse IgG

antibody (1:500, A-11034 or A-11019, Thermo Fisher Scientific) diluted in the same buffer at room temperature for 1 h. Cell nuclei were counterstained using VectaShield Mounting Medium with DAPI (Vector Laboratories). Fluorescence images were acquired using a Keyence BZ-9000 epifluorescence microscope equipped with a 4× or 40× objective.

QUANTIFICATION AND STATISTICAL ANALYSIS

ROI selection

A total of 50 ROIs were defined bilaterally (25 ROIs for each hemisphere) so that they covered all the cortical subregions designated in a dorsal cortical map[55,56] (Figure 1G). During our preliminary analysis, we visually inspected sample fluorescence movies of spontaneous cortical activity from three mice and selected several tens of ROI candidates that appeared brighter or darker than their surrounding regions. We then carefully examined and modified them so that the entire ROI set accords well with known cortical parcellations provided by annotated brain atlases.[55,56] The resultant ROI map was registered with fluorescence images of the dorsal cortex by manual translation and rotation so that Bregma and the midline of the ROI map and fluorescence images were in register. Each ROI was defined as a square of 5 × 5 pixels (within 128 × 128 pixel images) to avoid potential signal contamination across areal borders. In some cases, multiple ROIs assigned to relatively large cortical areas (e.g., primary somatosensory cortex, visual cortex, etc.) were arranged so that each corresponded to anatomical/functional subdivisions designated in the brain atlases.

The validity of our ROI positions for the primary somatosensory and primary visual cortices was confirmed by mapping sensory responses (Figure S1A). An air-puff (20 psi, 200 ms duration, PLI-10, Warner Instruments) to the right whiskers, forelimb, hindlimb, or the right side of the trunk and a flash of a yellow LED (0.2 Hz, 5 ms duration, Spectralynx, Neuralynx) to the right eye were given to mice anesthetized with 1.0–1.2% isoflurane as tactile and visual stimuli, respectively, and the areas that displayed the largest average fluorescence changes calculated from 25 to 30 responses were compared to the corresponding ROIs. The validity of ROI positions for motor areas was confirmed by constructing a pixel-based correlation map between fluorescence changes of the pixel and locomotor activity (Figures S1B and S1C). The consistency of ROI registration processes within and across genotypes was validated by consistent positions of multiple ROIs that corresponded to the primary somatosensory subareas (n = 9–11 Emx1G6 mice and 4–5 Emx1G6$_{15q\ dup}$ mice; Figure S6).

Data analysis

For locomotion analysis, the locomotion speed recorded at 60 Hz was downsampled to 30 Hz to match the timing of image acquisition. Periods of locomotion were defined as those during which the locomotion speed exceeded 0.5 cm/s, and the other periods were defined as those of rest. Episodes of locomotion and rest equal to or longer than 3 s were labeled as ''long locomotion'' and ''long rest,'' respectively. The remaining episodes were categorized as ''short locomotion'' and ''short rest.'' The threshold of 3 s was close to the average lengths of all locomotion and rest episodes (locomotion, 3.7 ± 7.3 s; rest, 2.6 ± 6.4 s; mean ± SD, n = 89 sessions) and was chosen to obtain a sufficient number of transition events per session (locomotion onset, 6.4 ± 3.9 events/session; locomotion cessation, 7.3 ± 4.7 events/session; mean ± SD, n = 89 sessions) while excluding periods of frequent alterations of the behavioral state that were too short to be used for the subsequent analysis of functional connectivity (FC) (Figure 1E). The exclusion of these periods did not likely affect the comparisons between Emx1G6 mice and Emx1G6$_{15q\ dup}$ mice, as stereotypy measured in an open-field test,[57] and the percentages of time spent on short locomotion and short rest were comparable between these genotypes (Figure 6C).

Raw fluorescence movies were spatially binned to 128 × 128 pixels and registered manually using ImageJ (NIH) so that the cortical image was aligned to a representative overhead view of the dorsal cortex.[55] Subsequent analyses were conducted using custom software written in MATLAB (Mathworks). Fluorescent intensities of the pixels within an ROI were averaged to represent the signal of the ROI, denoted F, and this value was divided by the baseline signal value $F0$, which was calculated as an average of F across all frames, to obtain normalized fluorescence changes $dF/F = (F\text{-}F0)/F0$.

The extent of fluorescence signals derived from intrinsic sources (flavin fluorescence and hemodynamics[58–60]) was estimated via the following two control experiments: imaging non-GCaMP6-expressing C57BL/6 (non-G6) mice (Figure S2) and correction of hemodynamic signals using two-wavelength imaging (Figure S5). In the former approach, basal fluorescence images of the dorsal cortical surface were acquired from non-G6 mice in order to estimate a potential upper bound of signal contamination. The average baseline signal intensity of non-G6 mice across three representative ROIs (M2a, HLp, and V1a) was 41.1 ± 0.9% of that in Emx1G6 mice (Figure S2B, mean ± SEM, n = 7 Emx1G6 mice and 3 non-G6 mice). Furthermore, the average fluorescence changes of non-G6 mice across all hemispheric ROIs after locomotion onset was 19.4 ± 2.2% of Emx1G6 mice (mean ± SEM, Figures S2C and S2D). These results imply that intrinsic fluorescence signals are much weaker and less dynamic than GCaMP fluorescence and that they constitute at most ∼8% of signal changes observed in Emx1G6 mice. These observations are consistent with other recent studies[61,62] that were conducted without compensation of endogenous signals.

In the latter approach, we imaged Ca^{2+}-dependent and -independent fluorescence signals at 470 and 405 nm wavelengths, respectively, in a separate cohort of Emx1G6 mice (n = 6), by following the previously described procedure.[63] Images of fluorescence excited at 470 and 405 nm were captured alternately at an overall frame rate of 40 frames per second (20 frames per second for each wavelength) using two LED drivers (470 nm, SOLIS-470C and DC20; 405 nm, M405L4 and LEDD1B, Thorlabs) controlled by custom LabVIEW software. A hemodynamic correction was conducted by subtracting $dF/F_{405\ nm}$ from $dF/F_{470\ nm}$, where $dF/F_{405\ nm}$ and $dF/F_{470\ nm}$ are

normalized fluorescence changes for signals obtained at 405 and 470 nm, respectively[64] (Figure S5A). The results demonstrate that although correlation coefficients between ROIs appeared slightly higher and thus resulted in identifying a larger number of highly correlated FCs (Figure S5B, see also Figure 2B), overall patterns of the network properties (node degree, betweenness centrality, CPL, and modularity Q, see below for details of these parameters) were qualitatively similar to those obtained without hemodynamic correction[34] (Figures S5C–S5F, see also Figure 2C–2F).

In this study, we focused on analyses of the dynamics of functional cortical networks during transitions between locomotion and rest. In the analysis of FC, we considered only transitions from long rest to long locomotion (locomotion onset) and those from long locomotion to long rest (locomotion cessation) (Figures 2, 3, and 6). This transition period also ensured that the comparison between Emx1G6 mice and Emx1G6$_{15q\ dup}$ mice was based on the data from time periods with identical motor features. As a control, we randomly selected reference time points regardless of the behavioral state as many times as an average number of locomotion onset and locomotion cessation (random control). Sessions with at least two onset or two cessation events were included for analysis, and average fluorescence changes across all onset, cessation, or random events were calculated to obtain values representative of each session. The numbers of each type of transitions (onset, cessation, and random, respectively) analyzed are as follows: Emx1G6, 566, 643, and 659 events, n = 89 sessions from 7 mice; no projection, 378, 447, and 451 events, n = 71 sessions from 17 mice; hemodynamics correction, 651, 612, and 656 events, n = 71 sessions from 6 mice; Emx1G6$_{15q\ dup}$, 268, 294, and 331 events, n = 88 sessions from 9 mice; Non-G6, 513, 621 and 590 events, n = 41 sessions from 3 mice.

To analyze FC between ROIs, we created correlation matrices representing the correlation between the cortical activity of all ROI pairs. We extracted 6-s segments of dF/F that spanned −3 s to +3 s around the event of interest (i.e., onset, cessation, or random). Each of the 6-s segments was further divided into 6 non-overlapping 1-s subsegments, and FC was calculated as pairwise Pearson correlation coefficients between dF/F during these 1-s subsegments. The 1-s time window was chosen to investigate rapid and dynamic changes of FC associated with behavior. In our initial analysis, we calculated correlations between ROI pairs using different time windows ranging from 0.33 s (10 frames) to 2 s (60 frames). This analysis revealed a tendency that the median correlation coefficients for all ROI pairs increases as the time window becomes longer. We selected the time window of 1 s as optimal because it was about in the middle of the linear range of the time window-correlation coefficients relationship (0.33 s, 0.681 ± 0.020; 0.67s, 0.689 ± 0.029; 1 s, 0.701 ± 0.034; 1.33 s, 0.725 ± 0.047; 1.67 s, 0.737 ± 0.040; 2 s, 0.744 ± 0.037; mean ± SD, n = 6 data points that correspond to the time windows −3, −2, −1, 1, 2, 3 in Figure 2B) and thus considered to be most sensitive to the changes in both positive and negative directions. The selection of the 1-s time window also accorded with the recent notion that spontaneous behavior and ongoing brain activity are related to each other at a timescale of about 1 s.[65] The correlation matrices obtained were averaged within a session and visualized as functional connectivity graphs of binarized networks using available MATLAB codes,[66] in which the positions of ROIs were arranged according to their anatomical positions, and lines and symbol sizes represented highly correlated FC ($r > 0.8$) and the number of such connections associated with the ROI, respectively. The threshold for binarization ($r > 0.8$) selected the top 26.7 ± 10.1% of the most prominent connections out of all 1,225 connections between 50 ROIs (mean ± SD, n = 1,602 subsegments from 89 sessions times 3 conditions; average correlation coefficient, onset, 0.68 ± 0.03; cessation, 0.68 ± 0.01; random, 0.68 ± 0.01; mean ± SD, n = 534 subsegments from 89 sessions). Node degree, betweenness centrality, characteristic path length (CPL), and modularity Q were calculated using the Brain Connectivity Toolbox.[21] Node degree and betweenness centrality represent the number of functional connections associated with each cortical ROI and the extent to which the ROI falls on the shortest paths between any other pairs of ROIs in the network, respectively. CPL represents the average shortest path length between all ROI pairs in the network. Modularity Q represents an index of optimized modules that maximize the number of within-module edges and minimize the number of between-module edges.

Support vector machine classification

Support vector machine (SVM) classification was performed using the Statistics and Machine Learning Toolbox in MATLAB. For behavior state classification, we used the "fitclinear" function to train a linear classification model with high-dimensional predictor data. The SVM was regularized by the lasso method to reduce model complexity and prevent overfitting. The FC datasets included 17,970-time point data that spanned the entire 10-min sessions. Each time point data contained 1,225 FCs from 50 ROIs as features. In the classification presented in Figure 5A, the FCs were calculated using a 1-frame sliding window of 30-frame size without excluding short locomotion and short rest periods. The corresponding behavioral data were binary vectors in which rest and locomotion were labeled as 0 and 1, respectively. Data that contained at least two episodes of long locomotion or long rest within a session were used. All relevant data (11–15 sessions per mouse) from each mouse were concatenated to be used for training and testing. An SVM classifier was trained using datasets from four of all seven mice (train set), and binary classification was conducted on each time point of the FC data from the remaining three mice (test set). All 35 combinations arising from seven mice ($_7C_4$) were tested. Accuracy was calculated as a percentage of time points that were classified to the right behavioral state. The chance level was defined as the overall average percentage of short and long locomotion periods (58%) since SVM tends to classify data into the more frequent category. In control, the datasets used for training were also used for testing ("train" control). In shuffled control, elements of behavioral state vectors were randomly shuffled and used for training and testing.

To identify features that contributed to the classification, we sorted features of the trained classifiers by their weights that represented coefficients of normal vector on the hyperplane. We then counted the appearance of features that included each ROI in the top 0.5% and bottom 0.5% distributions (6 features each, 12 total) as an importance index for the ROI. When cortical areas of interest

contained multiple ROIs, this index was normalized by their number. The chance level was defined as an average of 100 times random sampling. We then newly trained SVM classifiers using these top 0.5% and bottom 0.5% features and classified the test datasets to confirm that the selected features contribute to the classification. As a control, we tested classifiers trained with the same number of randomly selected features. This was repeated 100 times, and the results were averaged.

For genotype classification, we used the ''fitcsvm'' function in MATLAB, which trains and cross-validates an SVM model to solve problems with low-dimensional predictors. The 1,225 correlation coefficients were averaged throughout a session at each time point within relevant behavioral states or transitions. The data were then concatenated together for all relevant sessions, and the correlation coefficients were normalized into z-scores. We then cross-validated the classifiers using the leave-one-subject-out method, in which a pair of datasets from a mouse per each genotype were excluded from training and used for testing. In training, the classifiers were subjected to 10-fold cross-validation. All 63 combinations were tested from nine Emx1G6$_{15q\ dup}$ mice and seven Emx1G6 mice.

Statistics

To statistically test functional network connectivity, we used Network Based Statistic (NBS) Toolbox in MATLAB.[23] NBS nonparametrically calculates familywise error rate-corrected p-values with 5,000 times permutation testing. Inter-areal activity in test conditions was considered significantly correlated or decorrelated if the correlation coefficient during the behavioral transitions was higher or lower than random control with $p < 0.01$. In comparison between Emx1G6 mice and Emx1G6$_{15q\ dup}$ mice, the differences were considered significant when $p < 0.05$. Other statistical tests were performed using MATLAB or R. For two-group comparisons, Welch's t test was used when normal distributions were assumed. Otherwise, Wilcoxon rank-sum test was used. For comparisons between more than two groups, Wilcoxon rank-sum test with Bonferroni correction, one-way ANOVA and two-way ANOVA with Tukey-Kramer test were used.